ISSN 1450-7404

Journal of Research in Physics

Volume 34
Number 1
2010

DEPARTMENT OF PHYSICS

Faculty of Sciences
University of Novi Sad - Novi Sad - Serbia

Journal of Research in Physics

Published by: Department of Physics, Faculty of Sciences, University of Novi Sad,
Trg Dositeja Obradovića 4, 21000 Novi Sad, Serbia

Phone: +381-21-455318 Fax: +381-21-459367 E-mail: jresphys@df.uns.ac.rs
http://www.df.uns.ac.rs

Journal of Research in Physics Vol. 34, No. 1, 1 - 21 (2010)

Addition to the Theory of Liquid Phase Epitaxial Growth. II Crystallization Mechanisms

Nikolay Peev
Acad. G. Nadjakov Institute of Solid State Physics,
Bulgarian Academy of Sciences,
72 Tzarigradsko Chaussee blvrd, 1784 Sofia, Bulgaria

Received: *September 10, 2010*

Abstract

The work considers the possibility of determination of the crystallization mechanisms in the liquid phase epitaxial growth. On the basis of the components distribution and their behavior in the liquid phase, established in previous works, it was investigated how the epitaxial growth occurs in the case of different LPE growth techniques. The approach is based on the investigations of how the crystal growth rate depends on the cooling rate. It has been shown that in the case of normal growth mechanism the growth rate depends linearly on the cooling rate. In the case of screw dislocations growth mechanism this dependence is parabolic. This approach allows one to clearly distinguish the normal growth mechanism from that of screw dislocations growth. The two-dimensional nuclei growth can not be established by this approach. In this case the mode of the dependence of the growth rate on the cooling rate can not be derived analytically, which hinders the determination of this crystallization mechanism.

Key words: liquid phase epitaxy, crystallization mechanisms, LPE growth techniques

1. Introduction

The crystal growth processes are generally classified into two groups: gas phase methods and liquid phase methods, depending on the phase the transition is carried out. The most widely used gas phase epitaxial methods are Molecular Beam Epitaxy (MBE), Metallo-Organic Chemical Vapor Deposition (MOCVD) and Atomic Layer Epitaxy (ALE). These methods allow one to grow on a large substrate area of many epitaxial layers in only one process. This is the main advantage of the gas phase epitaxial methods. The main advantages of the Liquid Phase Epitaxy (LPE) methods are the high quality of the grown material in scope of structural perfection and electro-physical properties of the layer. Because of that for some materials oxides, garnets, high temperature superconductors [1-14] their use is preferable. The growth of very thin layers by LPE is quite possible - layers with thickness of about $50 - 100$ Å are successfully grown [16-19]. Nowadays, there are

developed LPE methods allowing the growth of layers onto a 3 inches wafer [9]. Concerning the single crystal growth, the liquid phase methods are preferable [13-15]. All of these circumstances show that the liquid phase growth methods are still very important and there are many other ways to improve them. Because of that their study and elaboration are still actual.

Three crystallization mechanisms of crystal growth are known: normal mechanism of growth, growth by screw dislocations, and growth by two-dimensional nuclei [20-23, 28]. The normal mechanism of growth takes place when onto the phase boundary a large amount of crystals growth steps is continuously available and the ad-atoms may incorporate into the crystal almost immediately. If the growth steps are not sufficient, the growth process can be assisted by the steps of the screw dislocations, permanently available on the crystal surface. If the above requirements are not fulfilled, then the crystal growth occurs by formation of two-dimensional nuclei onto the phase boundary. During migration on the crystal surface the ad-atoms form two-dimensional nuclei, which serve as crystal growth steps. The different mechanisms of growth in different manner depend on the supersaturation [20-23, 28].

Depending on the manner of how the supersaturation has been created, there are different LPE techniques: supercooling technique, equilibrium cooling technique, step cooling technique and transient cooling technique [11, 24-28]. The last two modes are alike - the growth temperature is constant and the liquid phase is preliminarily supercooled. Because of that they will be in the sequel called 'step cooling technique'.

Starting from the previously established effects [27-31, 34], the aim of the present work was to find out relations that would allow the determination of the crystal growth mechanism. In previous investigations [34] the effect of the initial supersaturation ΔC_{i0}^{L} on the growth rate v_{gr} was discussed with the aim to determine the crystallization mechanism. This approach is applicable only for the step cooling and supercooling techniques. However, it can not be applied for the equilibrium cooling technique, because no initial supercooling is needed there.

2. Theory

The case of n-component solid phase grown from n-component liquid phase is considered. We assume that the evaporation of the liquid phase is negligible. No chemical reactions and no convective mass transport take place in the liquid phase. The mass of the components passing from the liquid to the solid phase and forming the epitaxial layer is dm_i^L. This mass is always equal to the mass incorporated into the grown layer dm_i^S: $dm_i^S = -dm_i^L$. The solid phase has a constant composition, determined by the stochiometry of the grown compound. Thus, the change of mass of the components in the liquid phase correlates exactly with the stochiometry of the grown compound [27-31]:

$$\frac{dm_i^L}{M_i g_i} = \frac{dm_j^L}{M_j g_j}. \tag{1}$$

M_i and M_j are the atomic masses of the corresponding components, g_i and g_j are their stochiometry coefficients in the grown compound. Equation (1) provides relation between the changes of the masses dm_i^L of the components in the liquid phase within a time interval dt, and they must strongly correlate with the stochiometry of the grown compound.

The equilibrium concentration follows closely the temperature of the system:

$$dC_{i.eq}^{L} = \frac{dT}{k_i} = \frac{v_T dt}{k_i}, \tag{2}$$

where k_i is the slope of the liquidus surface with respect to the i-component: $k_i = dT/dC_{i.eq}^{L}$.

During the growth, the change of the actual concentration dC_i^L of an arbitrary i-component and the change of the mass dm_k^L of the basic k-component within the time dt correlate as follows [27-31]:

$$dC_i^L = \frac{C_k^L}{C_k^S}\left(C_i^S - C_i^L\right)\frac{dm_k^L}{m_k^L}, \tag{3}$$

where k is an arbitrary component of the system used as basic [27-31]. The notations used here are introduced in previous works [27-31, 34]. By the subscript "i" are denoted those components for which the concentration in the solid phase exceeds the concentration in the liquid phase: $C_i^S > C_i^L$. During the growth, the liquid phase depletes with time in respect to these components - their concentration C_i^L in the liquid phase decreases in consequence of crystallization [27, 28]. By the subscript "j" are denoted those components for which the concentration in the liquid phase exceeds that in the solid phase: $C_i^L > C_i^S$. During the growth, the liquid phase enhances in respect to these components - their concentration increases in consequence of crystallization.

In the present work, only the case of i-component is considered. Nevertheless, the relations derived are valid for the j-components. It is worth to be mentioned that in the term $(C_i^S - C_i^L)$ of equation (3) the order of the two concentrations has been changed compared to that in the previous works [29]. It is so because the decrease of the concentration C_i^L with time has been taken into account previously by a minus sign.

3. Stationary Growth Process

Stationary growth is possible only in the case of equilibrium cooling technique and in the supercooling technique. In the step cooling technique it is not possible, because of the peculiarities of the process - the growth takes place at a constant temperature, with preliminary supercooling, and the process is unsteady all the time.

During stationary growth, the supersaturation above the phase boundary remains constant. It means that the rise of the supersaturation due to the temperature cooling is fully compensated for by the crystallization process. In other words, within the time dt, the decrease of the equilibrium concentration $dC_{i.eq}^L$ due to the cooling (given by equation (2)) must be fully compensated for by the decrease of the actual concentration dC_i^L due to the layer deposition (given by equation (3)). It is worth to be pointed out that in equation 3 the change of the actual concentration dC_i^L depends on the growth rate $v_{\rm gr}$ through the change of the mass dm_i^L: $v_{\rm gr} \approx dm_i^L/dt$ [27, 29]. The equality of both equations ((2) and (3)) leads to the following relation, valid for the stationary growth regime:

$$\tilde{v}_{\rm gr} = \frac{M_0 \tilde{m}_k^L}{\gamma_0^S M_i g_i k_i}\frac{C_k^S}{\tilde{C}_k^L\left(C_i^S - \tilde{C}_i^L\right)}v_T. \tag{4}$$

A linear relation between the growth rate and the cooling rate is observed in case of stationary growth. By $\tilde{C}$, $\tilde{m}$ and $\tilde{v}$ are denoted the stationary values of the concentration, of the mass and of the growth rate respectively. Equation (4) coincides exactly with the expression obtained in another way in [34], concerning the stationary regime of growth.

4. Transient Growth Process

The crystal growth is governed mainly by two processes: 1) the diffusive mass transport of the components through the volume of the liquid phase, and 2) the surface kinetics of the atoms adsorbed onto the crystal surface till their incorporation into the crystal (into the kinks of the crystal edges, available continuously on the phase boundary). The growth rate is determined by the slower of the two processes. In the case of a diffusion limited growth, the concentration gradient and the diffusion coefficient determine the growth rate. In the case of growth limited by the surface kinetics, the rate is determined by the density of the growth steps (the kinks available along the crystal edges) and by the surface migration rate of the adsorbed particles.

In some LPE methods, it is not difficult to determine the growth regime. For example, in the case of temperature gradient zone melting it is well known that for thick zones the growth rate is determined by the diffusive mass transport and vice versa - the use of thin zones leads to a kinetics limited growth [32, 35]. In this way, the effect of the zone thickness l_0 on the growth rate v_{gr} provides information about the zone migration regime.

At the beginning of growth, the process is unsteady. If the process starts with preliminary supercooling ($\Delta C_{i0}^{L} \neq 0$), the actual concentration initially (at $t = 0$) exceeds greatly the equilibrium one. The initial supercooling enables a growth rate unattainable for the diffusive mass transport, because just at the beginning the concentration gradient is almost zero. During this period, the growth rate is much greater than the stationary one. In the phase boundary region, there is plenty matter to enable a high growth rate (the actual concentration exceeds much the equilibrium one). Because of that, the diffusive mass transport can not limit the growth rate. During this period, the growth rate will be limited by the phase boundary kinetics.

If the growth is carried out by equilibrium cooling technique, no initial supercooling is available: $\Delta C_{i0}^{L} = 0$ at $t = 0$. In consequence of the cooling, the liquid phase becomes supersaturated and the growth starts. At the beginning, the supersaturation is negligible - much lower than the stationary one. The growth rate is very slow - for keeping up the growth process a very slight mass transport is needed. The mass transport does not limit the growth process and the growth rate is determined by the surface kinetics again.

Hence, during the transient regime the growth is limited by the surface kinetics and, consequently, it provides information concerning the crystal growth mechanism. Because of that, the knowledge of how the transient process occurs, is very important.

With this aim, the growth time has been split into very small intervals δt. During these periods the quantities C_i^L, C_k^L, m_k^L, k_i, v_T, $C_{i.eq}^L$ are assumed to remain constant. The end values of the equilibrium and actual concentrations and the growth rate within the intervals were determined by equations (2) and (3). The obtained end values are used as initial values for the next step, concerning the next time interval. In this way, the transient process may be studied.

Firstly, the supercooling technique is considered, because all the others can be derived

from this technique. The equilibrium cooling technique may be derived from the supercooling technique by setting the preliminary super saturation to be zero ($\Delta C^L_{i0} = 0$). The step cooling technique one may obtain from the supercooling technique at zero cooling rate ($v_T = 0$).

4.1. Supercooling Technique

In the case of supercooling technique, the liquid phase is initially supersaturated: $\Delta C^L_i(t = 0) = \Delta C^L_{i0} = C^L_{i0} - C^L_{i.eq0}$. Simultaneously with bringing the two phases into contact (at $t = 0$) the cooling starts and the growth begins. At the end of the first interval δt the temperature of the system will be: $T(\delta t) = T_0 - v_T \delta t/k_{i1}$ (Figure 1). The equilibrium concentration is lowered to the value $C^L_{i.eq}(\delta t) = C^L_{i.eq1} = C^L_{i.eq0} - v_T \delta t/k_{i1}$. In consequence of crystallization, the true concentration of the i-component decreases in accordance with equation (3):

$$\begin{aligned} C^L_i(\delta t) &= C^L_{i1} = C^L_{i0} - \delta C^L_{i1} = \\ &= C^L_{i0} - \frac{\gamma^S_0 M_i g_i}{M_0 m^L_{k0}} \frac{C^L_{k0}}{C^S_k} \left(C^S_i - C^L_{i0} \right) v_{gr1} \delta t. \end{aligned} \tag{5}$$

For the supersaturation one obtains:

$$\begin{aligned} \Delta C^L_i(\delta t) &= \Delta C^L_{i1} = C^L_{i1} - C^L_{i.eq1} = \\ &= \Delta C^L_{i0} + \frac{v_T \delta t}{k_{i1}} - \frac{\gamma^S_0 M_i g_i}{M_0 m^L_{k0}} \frac{C^L_{k0}}{C^S_k} \left(C^S_i - C^L_{i0} \right) v_{gr1} \delta t. \end{aligned} \tag{6}$$

In this case the supersaturation decreases initially to its stationary value $\Delta C^L_{i.st}$ and then remains constant (Figure 1). In equation (6), the growth rate $v_{\rm gr}$ depends also on the supersaturation ΔC^L_i. For the different mechanisms of growth, the growth rate depends in a different manner on the supersaturation.

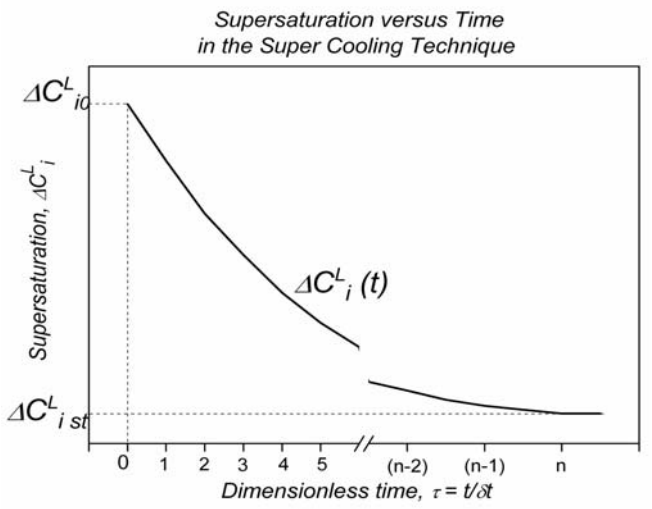

Figure 1. Supersaturation versus time for the supercooling technique.

4.1.1. Normal Growth Mechanism

In this case the growth rate depends on the supersaturation linearly:

$$v_{gr} = \mu"_i \Delta T = \mu"_i k_i \Delta C_i^L. \tag{7}$$

ΔC_i^L is the supersaturation just above the phase boundary, which determines the growth rate. By equations (6) and (7) one obtains the value of ΔC_{i1}^L:

$$\begin{aligned} \Delta C_{i1}^L &= \frac{A_{i1}}{1+B_{i1}} = \frac{\Delta C_{i0}^L + \dfrac{v_T \delta t}{k_{i1}}}{1 + \dfrac{\gamma_0^S M_i g_i}{M_0 m_{k0}^L} \dfrac{C_{k0}^L}{C_k^S} \left(C_i^S - C_{i0}^L\right) \mu"_{i1} k_{i1} \delta t}, \\ A_{i1} &= \Delta C_{i0}^L + \frac{v_T \delta t}{k_{i1}}; \qquad B_{i1} = \frac{\gamma_0^S M_i g_i}{M_0 m_{k0}^L} \frac{C_{k0}^L}{C_k^S} \left(C_i^S - C_{i0}^L\right) \mu"_{i1} k_{i1} \delta t. \end{aligned} \tag{8}$$

Using the value of ΔC_{i1}^L from equation (8) one determines the true concentration at $t = \delta t$. It is the initial value for the next time interval. In the same way one may investigate the system in the time interval $t \in (\delta t, 2\delta t)$. For the n-th interval δt (at $t = n\delta t$) one obtains:

$$\begin{aligned} \Delta C_{in}^L &= \frac{A_{in}}{1+B_{in}} = \frac{\Delta C_{in-1}^L + \dfrac{v_T \delta t}{k_{in}}}{1 + \dfrac{\gamma_0^S M_i g_i}{M_0 m_{kn-1}^L} \dfrac{C_{kn-1}^L}{C_k^S} \left(C_i^S - C_{in-1}^L\right) \mu"_{in} k_{in} \delta t}, \\ A_{in} &= \Delta C_{i0}^L + \sum_{j=1}^{n} \frac{v_T \delta t}{k_{ij}} - \sum_{j=1}^{n-1} \frac{\gamma_0^S M_i g_i}{M_0 m_{kj-1}^L} \frac{C_{kj-1}^L}{C_k^S} \left(C_i^S - C_{ij-1}^L\right) \mu"_{ij} k_{ij} \Delta C_{ij}^L \delta t = \\ &= \Delta C_{in-1}^L + \frac{v_T \delta t}{k_{in}}; \\ B_{in} &= \frac{\gamma_0^S M_i g_i}{M_0 m_{kn-1}^L} \frac{C_{kn-1}^L}{C_k^S} \left(C_i^S - C_{in-1}^L\right) \mu"_{in} k_{in} \delta t. \end{aligned} \tag{9}$$

During the n-th interval the regime of transient growth is up (as shown on Figure 1), the system goes over to stationary growth. Then the equality $\Delta C_{in-1}^L = \Delta C_{in}^L$ must be valid, and from equations (7) and (9) follows exactly equation (4), holding for the stationary growth.

4.1.2. Screw Dislocations Growth Mechanism

In this case the growth rate depends by a quadratic relation on the supersaturation [20, 32, 35]:

$$v_{gr} = \mu_i k_i^2 \left(\Delta C_i^L\right)^2. \tag{10}$$

By expressions (10) and (6) one obtains a quadratic equation concerning the supersaturation ΔC_{i1}^L:

$$
\begin{aligned}
H_{i1}{\Delta C_{i1}^L}^2 + \Delta C_{i1}^L - \left(\Delta C_{i0}^L + \frac{v_T \delta t}{k_{i1}}\right) = 0, \\
H_{i1} = \frac{\gamma_0^S M_i g_i}{M_0 m_{k0}^L} \frac{C_{k0}^L}{C_k^S} \left(C_i^S - C_{i0}^L\right) \mu_{i1} k_{i1}^2 \delta t.
\end{aligned}
\tag{11}
$$

The value of the supersaturation at the end of the time interval is as follows:

$$
\Delta C_{i1}^L = \left[-1 + \sqrt{1 + 4H_{i1}\left(\Delta C_{i0}^L + \frac{v_T \delta t}{k_{i1}}\right)}\right] \frac{1}{2H_{i1}}. \tag{12}
$$

The next time intervals are treated in a similar way. For the n-th interval one obtains the expression:

$$
\begin{aligned}
H_{in}{\Delta C_{in}^L}^2 + \Delta C_{in}^L - \left(\Delta C_{in-1}^L + \frac{v_T \delta t}{k_{in}}\right) = 0, \\
\Delta C_{in}^L = \left[-1 + \sqrt{1 + 4H_{in}\left(\Delta C_{in-1}^L + \frac{v_T \delta t}{k_{in}}\right)}\right] \frac{1}{2H_{in}}.
\end{aligned}
\tag{13}
$$

$$
H_{in} = \frac{\gamma_0^S M_i g_i}{M_0 m_{kn-1}^L} \frac{C_{kn-1}^L}{C_k^S} \left(C_i^S - C_{in-1}^L\right) \mu_{in} k_{in}^2 \delta t. \tag{14}
$$

In the case of stationary growth ($\Delta C_{in-1}^L \equiv \Delta C_{in}^L$), from equation (13) one obtains again equation (4), by taking into account equation (10).

4.1.3. Two-dimensional Nuclei Growth

In the case of two-dimensional nuclei growth the growth rate depends on the supercooling by an exponential relation [32, 35]:

$$
v_{\mathrm{gr}} = \mu' exp\left(\frac{\pi \lambda \sigma_{sl}^2 v_T T}{k_B \Delta H T_{eq} \Delta T}\right). \tag{15}
$$

μ' is the kinetic coefficient, characterizing the processes of two-dimensional nuclei formation, taking place on the phase boundary. λ is the elementary jump of the particles toward the crystal surface within the interface region. The particle adsorbs onto the crystal surface and migrating over it, forms with the other particles a two-dimensional nucleus. σ_{sl} is the surface tension at the phase boundary liquid-solid, v_T is the cooling rate, T, T_{eq}, ΔT are the true temperature, the equilibrium temperature and the supercooling respectively: ($T_{eq} = T + \Delta T$). ΔH is the value of the enthalpy of the phase transition that takes place,and k_B is the Boltzmann constant. Equation (15) can be rewritten in the following

form:

$$\begin{aligned} v_{\rm gr} &= \mu' exp\left(\frac{A}{T}\right) exp\left(-\frac{A}{\Delta T}\right), \\ A &= \frac{\pi\lambda\sigma_{sl}^2 v_T}{k_B \Delta H}. \end{aligned} \tag{16}$$

At the end of the first time interval the value of the equilibrium concentration will be: $C^L_{i.eq}(\delta t) = C^L_{i.eq1} = C^L_{i.eq0} - v_T\delta t/k_{i1}$. The values of the actual concentration and the supersaturation are given by equations (5) and (6). By equations (6) and (16) one obtains the supersaturation ΔC^L_{i1}:

$$\begin{aligned} \Delta C^L_{i1} &= \Delta C^L_{i0} + \frac{v_T\delta t}{k_{i1}} - \frac{\gamma_0^S M_i g_i}{M_0 m^L_{k0}} \frac{C^L_{k0}}{C^S_k}\left(C^S_i - C^L_{i0}\right)\mu'_{i1} exp\left(\frac{A}{T_0}\right) exp\left(-\frac{A}{k_{i1}\Delta C^L_{i1}}\right)\delta t = \\ &= B^1_{i1} - B^1_{i2} exp\left(-\frac{A}{k_{i1}\Delta C^L_{i1}}\right), \\ & B^1_{i1} = \Delta C^L_{i0} + \frac{v_T\delta t}{k_{i1}}, \\ & B^1_{i2} = \frac{\gamma_0^S M_i g_i}{M_0 m^L_{k0}} \frac{C^L_{k0}}{C^S_k}\left(C^S_i - C^L_{i0}\right)\mu'_{i1} exp\left(\frac{A}{T_0}\right)\delta t, \\ & f_1 \equiv \Delta C^L_{i1} = B^1_{i1} - B^1_{i2} exp\left(-\frac{A}{k_{i1}\Delta C^L_{i1}}\right) \equiv f_2. \end{aligned} \tag{17}$$

In equation (17), T_0 is the initial value of the temperature. The epitaxial process usually occurs in a very small temperature interval, and because of that the quantities before the exponent may be considered as constants. Equation (17) may be solved in a graphic way. The point of intersection of the two functions f_1 and f_2 provides the value of ΔC^L_{i1}.

During the n-th δt-time interval the supersaturation is ΔC^L_{in}:

$$\begin{aligned} & \Delta C^L_i(n\delta t) = \Delta C^L_{in} = C^L_i(n\delta t) - C^L_{i.eq}(n\delta t) = B^n_{i1} - B^n_{i2} exp\left(-\frac{A}{k_{in}\Delta C^L_{in}}\right), \\ & B^n_{i1} = \Delta C^L_{i0} + \sum_{j=1}^{n} \frac{v_T\delta t}{k_{ij}} - \\ & - \sum_{j=1}^{n-1} \frac{\gamma_0^S M_i g_i}{M_0 m^L_{kj-1}} \frac{C^L_{kj-1}}{C^S_k}\left(C^S_i - C^L_{ij-1}\right)\delta t\mu'_{ij} exp\left(\frac{A}{T_0 - (j-1)v_T\delta t}\right) exp\left(-\frac{A}{k\Delta C^L_{ij}}\right), \\ & B^n_{i2} = \frac{\gamma_0^S M_i g_i}{M_0 m^L_{kn-1}} \frac{C^L_{kn-1}}{C^S_k}\left(C^S_i - C^L_{in-1}\right)\delta t\mu'_{in} exp\left(\frac{A}{T_0 - (n-1)v_T\delta t}\right). \end{aligned} \tag{18}$$

In the case of stationary growth, from equation (18) follows exactly equation (4), by taking into account equation (16). In all the next considerations equation (4) follows exactly, so that this fact will not be pointed out explicitly.

4.2. Equilibrium Cooling Technique

The crystal growth by this technique occurs at very small deviations from equilibrium - at the onset the true concentration is equal to the equilibrium one: $C^L_{i.eq0} = C^L_{i0}$ and $\Delta C^L_{i0} = C^L_{i0} - C^L_{i.eq0} = 0$. At $t = 0$ starts the cooling and the growth begins - in consequence of the cooling a supersaturation arises. The supersaturation increases with time continuously (Figure 2) - this is the transient growth regime. At the end of the transient growth, the supersaturation and the growth rate stop to increase and remain almost constant.

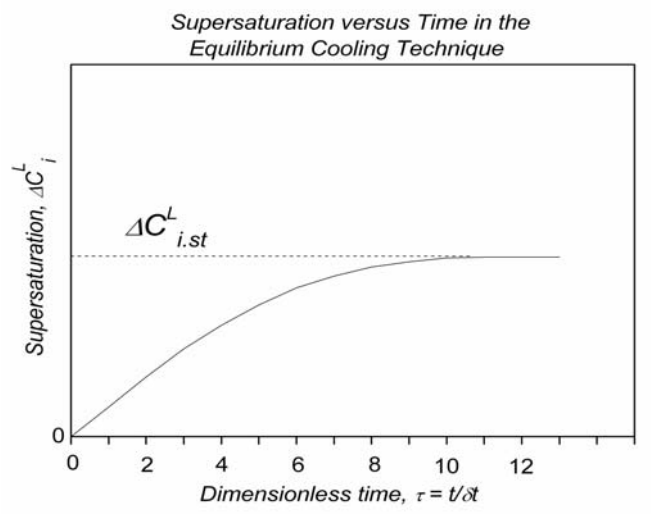

Figure 2. Supersaturation versus time for the equilibrium cooling technique.

By setting to zero the initial supersaturation ($\Delta C^L_{i0} = 0$), this epitaxial technique can be derived from the expressions of the supersaturation technique. Expressions for the equilibrium concentration, for the actual concentration and for the supersaturation are given below (equation (19)):

$$\begin{aligned} C^L_{i.eq}(\delta t) &= C^L_{i.eq1} = C_{i.eq0} - \frac{v_T \delta t}{k_{i1}}, \\ C^L_i(\delta t) &= C^L_{i1} = C^L_{i0} - \delta C^L_{i1} = C^L_{i0} - \frac{\gamma^S_0 M_i g_i}{M_0 m^L_{k0}} \frac{C^L_{k0}}{C^S_k} \left(C^S_i - C^L_{i0} \right) v_{\mathrm{gr}1} \delta t, \\ \Delta C^L_i(\delta t) &= \Delta C^L_{i1} = C^L_{i1} - C^L_{i.eq1} = \frac{v_T \delta t}{k_{i1}} - \frac{\gamma^S_0 M_i g_i}{M_0 m^L_{k0}} \frac{C^L_{k0}}{C^S_k} \left(C^S_i - C^L_{i0} \right) v_{\mathrm{gr}1} \delta t. \end{aligned} \tag{19}$$

At $\Delta C^L_{i0} = 0$ equations (6) and (7) coincide exactly with equations (19).

4.2.1. Normal Growth Mechanism

In this case the growth rate changes linearly with the supersaturation as already mentioned (equation (7)). By substituting equation (7) in (19) one obtains the value of the supersaturation ΔC^L_{i1} at the end of the first time interval $t = \delta t$:

$$\begin{aligned}
\Delta C_{i1}^L &= \frac{v_T \delta t}{k_{i1}} - \frac{\gamma_0^S M_i g_i}{M_0 m_{k0}^L} \frac{C_{k0}^L}{C_k^S} \left(C_i^S - C_{i0}^L \right) \mu"_{i1} k_{i1} \Delta C_{i1}^L \delta t = A'_{i1} - B'_{i1} \Delta C_{i1}^L, \\
&\Delta C_{i1}^L = \frac{A'_{i1}}{1 + B'_{i1}}, \\
&A'_{i1} = \frac{v_T \delta t}{k_{i1}} = A_{i1} - \Delta C_{i0}^L, \\
&B'_{i1} = B_{i1}.
\end{aligned} \tag{20}$$

The last equation follows exactly from equation (8) at $\Delta C_{i0}^L = 0$. The value of ΔC_{i1}^L allows the determination of the value of the true concentration. In this way, step by step one may examine the transient growth regime. For the n-th period one obtains the expression:

$$\begin{aligned}
\Delta C_{in}^L &= \frac{A'_{in}}{1 + B'_{in}} = \frac{\Delta C_{in-1}^L + \frac{v_T \delta t}{k_{in}}}{1 + \frac{\gamma_0^S M_i g_i}{M_0 m_{kn-1}^L} \frac{C_{kn-1}^L}{C_k^S} \left(C_i^S - C_{in-1}^L \right) \mu"_{in} k_{in} \delta t}, \\
&A'_{in} = \sum_{j=1}^{n} \frac{v_T \delta t}{k_{ij}} - \sum_{j=1}^{n-1} \frac{\gamma_0^S M_i g_i}{M_0 m_{kj-1}^L} \frac{C_{kj-1}^L}{C_k^S} \left(C_i^S - C_{ij-1}^L \right) \mu"_{ij} k_{ij} \Delta C_{ij}^L \delta t, \\
&B'_{in} = \frac{\gamma_0^S M_i g_i}{M_0 m_{kn-1}^L} \frac{C_{kn-1}^L}{C_k^S} \left(C_i^S - C_{in-1}^L \right) \mu"_{in} k_{in} \delta t \equiv B_{in}.
\end{aligned} \tag{21}$$

4.2.2. Screw Dislocations Growth Mechanism

With the aid of equations (10) and (21) one obtains a quadratic equation concerning the supersaturation:

$$\begin{aligned}
\Delta C_{i1}^L &= \frac{v_T \delta t}{k_{i1}} - \frac{\gamma_0^S M_i g_i}{M_0 m_{k0}^L} \frac{C_{k0}^L}{C_k^S} \left(C_i^S - C_{i0}^L \right) \mu_{i1} k_{i1}^2 {\Delta C_{i1}^L}^2 \delta t = \\
&= \frac{v_T \delta t}{k_{i1}} - H_{i1} {\Delta C_{i1}^L}^2.
\end{aligned} \tag{22}$$

The solution of the quadratic equation provides the value of ΔC_{i1}^L:

$$\Delta C_{i1}^L = \left(-1 + \sqrt{1 + 4 H_{i1} \frac{v_T \delta t}{k_{i1}}} \right) \frac{1}{2 H_{i1}}. \tag{23}$$

This is in fact equation (12) at no initial supersaturation: $\Delta C_{i0}^L = 0$. For the supersaturation during the n-th time interval one obtains the expression:

$$\begin{aligned}
\Delta C_{in}^L &= v_T \delta t \sum_{j=1}^{n} \frac{1}{k_{ij}} - \frac{\gamma_0^S M_i g_i}{M_0} \sum_{j=1}^{n} \frac{C_{kj-1}^L}{C_k^S} \left(C_i^S - C_{ij-1}^L \right) \frac{\mu_j}{m_{kj-1}^L} \left[\sum_{l=1}^{j} k_{il} \Delta C_{il}^L \right]^2 \delta t = \\
&= \Delta C_{in-1}^L + \frac{v_T \delta t}{k_{in}} - \frac{\gamma_0^S M_i g_i}{M_0 m_{kn-1}^L} \frac{C_{kn-1}^L}{C_k^S} \left(C_i^S - C_{in-1}^L \right) \mu_n \left[\sum_{l=1}^{n} k_{il} \Delta C_{il}^L \right]^2 \delta t \\
&\quad H_{in} {\Delta C_{in}^L}^2 + G_{in} \Delta C_{in}^L - D_{in} = 0,
\end{aligned} \tag{24}$$

where

$$\begin{aligned}
D_{in} &= v_T \delta t \sum_{j=1}^{n} \frac{1}{k_{ij}} - \frac{\gamma_0^S M_i g_i}{M_0} \sum_{j=1}^{n-1} \frac{C_{kj-1}^L}{C_k^S} \left(C_i^S - C_{ij-1}^L \right) \frac{\mu_j}{m_{kj-1}^L} \left[\sum_{l=1}^{j} k_{il} \delta \left(\Delta C_{il}^L \right) \right]^2 \delta t - \\
&- \frac{\gamma_0^S M_i g_i}{M_0} \frac{C_{kn-1}^L}{C_k^S} \left(C_i^S - C_{in-1}^L \right) \frac{\mu_n}{m_{kn-1}^L} \left[\sum_{j=1}^{n-1} k_{ij} \delta \left(\Delta C_{ij}^L \right) \right]^2 \delta t, \\
H_{in} &= \frac{\gamma_0^S M_i g_i}{M_0 m_{kn-1}^L} \frac{C_{kn-1}^L}{C_k^S} \left(C_i^S - C_{in-1}^L \right) \mu_n k_{in}^2 \delta t, \\
G_{in} &= 1 + 2 \frac{\gamma_0^S M_i g_i}{M_0 m_{kn-1}^L} \frac{C_{kn-1}^L}{C_k^S} \left(C_i^S - C_{in-1}^L \right) \mu_n k_{in} \sum_{j=1}^{n-1} k_{ij} \delta \left(\Delta C_{ij}^L \right) \delta t, \\
\Delta C_{in}^L &= \frac{1}{2H_{in}} \left(-G_{in} + \sqrt{G_{in}^2 + 4 D_{in} H_{in}} \right).
\end{aligned} \tag{25}$$

4.2.3. Two-dimensional Nuclei Growth

The relation between the growth rate and the supersaturation in this case is provided by equation (16). Substituting it into equation (19) one obtains expression for the supersaturation:

$$\Delta C_{i1}^L = \frac{v_T \delta t}{k_{i0}} - \frac{\gamma_0^S M_i g_i}{M_0 m_{k0}^L} \frac{C_{k0}^L \left(C_i^S - C_{i0}^L \right)}{C_k^S} \mu' exp \left(\frac{A}{T_0} \right) exp \left(-\frac{A}{k_{i1} \Delta C_{i1}^L} \right) \delta t. \tag{26}$$

The last equation may be solved graphically as already mentioned.

$$\begin{aligned}
f_{11} &= \Delta C_{i1}^L = B_{i1}^{1'} - B_{i2}^{1'} \exp \left(-\frac{A}{k_{i1} \Delta C_{i1}^L} \right) \equiv f_{21}, \\
&\quad f_{11} = \Delta C_{i1}^L; \qquad f_{21} = B_{i1}^{1'} - B_{i2}^{1'} \exp \left(-\frac{A}{k_{i1} \Delta C_{i1}^L} \right), \\
&\quad B_{i1}^{1'} = \frac{v_T \delta t}{k_{i1}} = B_{i1}^1 - \Delta C_{i0}^L, \\
&\quad B_{i2}^{1'} = \frac{\gamma_0^S M_i g_i}{M_0 m_{k0}^L} \frac{C_{k0}^L \left(C_i^S - C_{i0}^L \right) \delta t}{C_k^S} \mu_{i1}' exp \left(\frac{A}{T_0} \right) \equiv B_{i2}^1.
\end{aligned} \tag{27}$$

For the n-th time interval one obtains respectively:

$$\begin{aligned} f_{1n} \equiv \Delta C_{in}^{L} = B_{i1}^{n'} - B_{i2}^{n'} \exp\left(-\frac{A}{\sum\limits_{j=1}^{n} k_{ij}\Delta C_{ij}^{L}}\right) \equiv f_{2n}, \\ B_{i1}^{n'} = \Delta C_{in-1}^{L} + \frac{v_T \delta t}{k_{in}}, \\ B_{i2}^{n'} = \frac{\gamma_0^S M_i g_i}{M_0 m_{kn-1}^{L}} \frac{C_{kn-1}^{L}\left(C_i^S - C_{in-1}^{L}\right)\delta t}{C_k^S} \mu'_{in} exp\left(\frac{A}{T_0 - (n-1)v_T \delta t}\right). \end{aligned} \tag{28}$$

4.3. Step Cooling Technique

Before the growth is to start, the solid and the liquid phases are not in contact with each other. The liquid phase is supersaturated in respect to the solid phase: $\Delta T_0 = k_i \Delta C_{i0}^{L}$. Due to the preliminary supersaturation the growth process starts immediately with the contact between the two phases. The growth occurs at constant temperature. The stationary growth is not possible in this technique - the process is unsteady. The growth rate and the supersaturation change continuously with time, tending to zero (Figures 3-1 and 3-2).

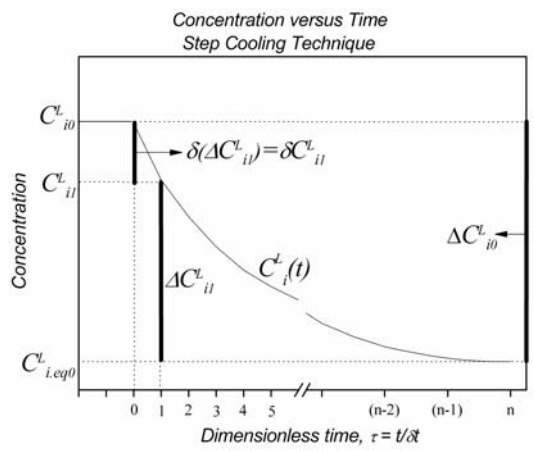

Figure 3-1. Concentration versus time for the step cooling technique.

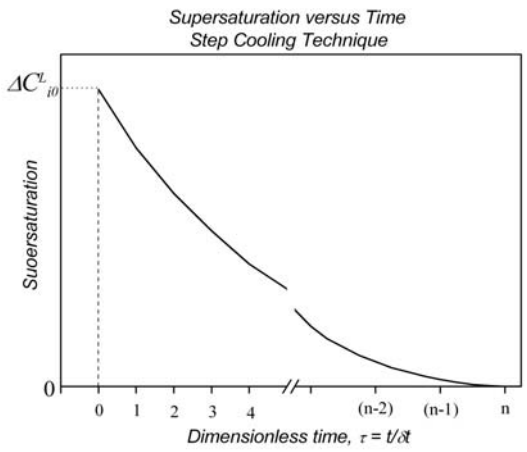

Figure 3-2. Supersaturation versus time for the step cooling technique.

If the contact between the two phases is long enough, the growth process terminates and the phases come to equilibrium. During the entire process, the equilibrium concentration remains constant (because of the constant temperature). Consequently, the change of the supersaturation is equal to the change of the true concentration: $\delta C_i^L \equiv \delta(\Delta C_i^L)$:

$$C_{i.eq}^{L}(t) = C_{i0}^{L} - \Delta C_{i0}^{L} = C_{i.eq0}^{L} = const. \tag{29}$$

$$C_{i1}^L = C_{i0}^L - \delta C_{i1}^L = C_{i0}^L - \frac{\gamma_0^S M_i g_i}{M_0 m_{k0}^L} \frac{C_{k0}^L}{C_k^S} \left(C_i^S - C_{i0}^L \right) v_{\mathrm{gr}1} \delta t. \tag{30}$$

The value of the supersaturation at the same time will be as follows:

$$\Delta C_i^L(\delta t) = \Delta C_{i1}^L = C_{i1}^L - C_{i.eq}^L = \Delta C_{i0}^L - \frac{\gamma_0^S M_i g_i}{M_0 m_{k0}^L} \frac{C_{k0}^L}{C_k^S} \left(C_i^S - C_{i0}^L \right) v_{\mathrm{gr}1} \delta t. \tag{31}$$

Relations for the step cooling technique may be obtained from the corresponding relations of the supercooling technique by setting the cooling rate to be equal to zero: $v_T = 0$.

4.3.1. Normal Growth Mechanism

Using equations (7) and (31), one obtains a linear expression concerning the supersaturation:

$$\begin{aligned} \Delta C_i^L(\delta t) \quad = \quad & \Delta C_{i1}^L = \Delta C_{i0}^L - \frac{\gamma_0^S M_i g_i}{M_0 m_{k0}^L} \frac{C_{k0}^L}{C_k^S} \left(C_i^S - C_{i0}^L \right) \mu^{"}{}_{i1} k_{i1} \Delta C_{i1}^L \delta t, \\ & \Delta C_{i1}^L = \frac{\Delta C_{i0}^L}{1 + \frac{\gamma_0^S M_i g_i}{M_0 m_{k0}^L} \frac{C_{k0}^L}{C_k^S} \left(C_i^S - C_{i0}^L \right) \mu^{"}{}_{i1} k_{i1} \delta t}. \end{aligned} \tag{32}$$

For the n-th interval one obtains:

$$\begin{aligned} \Delta C_{in}^L \quad = \quad & \Delta C_{in-1}^L - \frac{\gamma_0^S M_i g_i}{M_0 m_{kn-1}^L} \frac{C_{kn-1}^L}{C_k^S} \left(C_i^S - C_{in-1}^L \right) \mu^{"}{}_{in} k_{in} \Delta C_{in}^L \delta t, \\ & \Delta C_{in}^L = \frac{\Delta C_{in-1}^L}{1 + \frac{\gamma_0^S M_i g_i}{M_0 m_{kn-1}^L} \frac{C_{kn-1}^L}{C_k^S} \left(C_i^S - C_{in-1}^L \right) \mu^{"}{}_{in} k_{in} \delta t}. \end{aligned} \tag{33}$$

Equations (32) and (33) follow exactly from equations (8) and (9) at $v_T = 0$.

4.3.2. Screw Dislocations Growth Mechanism

By equations (10) and (31) one obtains the corresponding relations:

$$\begin{aligned}
\delta C_{i1}^L &= \delta\left(\Delta C_{i1}^L\right) = \frac{\gamma_0^S M_i g_i}{M_0 m_{k0}^L}\frac{C_{k0}^L}{C_k^S}\left(C_i^S - C_{i0}^L\right) v_{\mathrm{gr}1}\delta t = \\
&= \frac{\gamma_0^S M_i g_i}{M_0 m_{k0}^L}\frac{C_{k0}^L}{C_k^S}\left(C_i^S - C_{i0}^L\right)\mu_i k_{i1}^2\left[\Delta C_{i0}^L - \delta\left(\Delta C_{i1}^L\right)\right]^2\delta t = \\
&= H_{i1}\left[\Delta C_{i0}^L - \delta\left(\Delta C_{i1}^L\right)\right]^2, \\
&H_{i1}\left[\Delta C_{i0}^L - \delta\left(\Delta C_{i1}^L\right)\right]^2 + \left[\Delta C_{i0}^L - \delta\left(\Delta C_{i1}^L\right)\right] - \Delta C_{i0}^L = 0.
\end{aligned} \tag{34}$$

From the quadratic equation (34) one obtains the value of the supersaturation:

$$\Delta C_{i0}^L - \delta C_{i1}^L = \frac{1}{2H_{i1}}\left[-1 + \left(1 + 4H_{i1}\Delta C_{i0}^L\right)^{1/2}\right]. \tag{35}$$

For the n-th interval, the value of the supersaturation is as follows:

$$\begin{aligned}
\Delta C_{i0}^L - \sum_{j=1}^{n}\delta\left(\Delta C_{ij}^L\right) &= \Delta C_{in}^L = \\
&= \frac{1}{2H_{in}}\left\{-1 + \left[1 + 4H_{in}\left(\Delta C_{i0}^L - \sum_{j=1}^{n-1}\delta\left(\Delta C_{ij}^L\right)\right)\right]^{1/2}\right\}.
\end{aligned} \tag{36}$$

4.3.3. Two-dimensional Nuclei Growth

In this case equations (16) and (31) provide the expression:

$$\begin{aligned}
\Delta C_i^L(\delta t) &\equiv \Delta C_{i1}^L = C_{i1}^L - C_{i.eq0}^L = \Delta C_{i0}^L - \delta C_{i1}^L = \\
&= \Delta C_{i0}^L - \frac{\gamma_0^S M_i g_i}{M_0 m_{k0}^L}\frac{C_{k0}^L}{C_k^S}\left(C_i^S - C_{i0}^L\right) v_{\mathrm{gr}1}\delta t = \\
&= \Delta C_{i0}^L - \frac{\gamma_0^S M_i g_i}{M_0 m_{k0}^L}\frac{C_{k0}^L}{C_k^S}\left(C_i^S - C_{i0}^L\right)\mu_{i1}'\delta t exp\left(\frac{A}{T_0}\right) exp\left(-\frac{A}{k_{i1}\Delta C_{i1}^L}\right).
\end{aligned} \tag{37}$$

The supersaturation is determined graphically. For the n-th interval: $t \in [(n-1)\delta t, n\delta t]$ one obtains:

$$\begin{aligned}
\Delta C_{in}^L &= B_{i1}^{n"} - B_{i2}^{n"}\exp\left(-\frac{A}{k_{in}\Delta C_{in}^L}\right), \\
B_{i1}^{n"} &= \Delta C_{i0}^L - \sum_{j=1}^{n-1}\frac{\gamma_0^S M_i g_i}{M_0 m_{kj-1}^L}\frac{C_{kj-1}^L}{C_k^S}\left(C_i^S - C_{ij-1}^L\right)\mu_{ij}'\delta t exp\left(\frac{A}{T_0}\right) exp\left(-\frac{A}{k_{ij}\Delta C_{ij}^L}\right), \\
B_{i2}^{n"} &= \frac{\gamma_0^S M_i g_i}{M_0 m_{kn-1}^L}\frac{C_{kn-1}^L}{C_k^S}\left(C_i^S - C_{in-1}^L\right)\mu_{in}'\delta t exp\left(\frac{A}{T_0}\right).
\end{aligned} \tag{38}$$

5. Discussion

These considerations allow one to distinguish the normal growth mechanism from the screw dislocations growth mechanism. For this purpose, the knowledge of the function $v_{\rm gr}(v_T)$ is needed. The effect of the cooling rate v_T on the growth rate $v_{\rm gr}$ is substantially different for the two growth mechanisms. The effect depends on the used growth technique. In the case of two-dimensional nuclei growth the function $v_{\rm gr}(v_T)$ in analytic form is unknown - the problem is solved graphically. This circumstance hinders the determination of this mechanism of growth.

In the case of normal growth mechanism, the growth rate increases with the cooling rate linearly in any of the growth techniques. In the case of supercooling technique, by substituting the value of the supersaturation ΔC_{i1}^L from equation (8) into equation (7) for the growth rate one obtains:

$$v_{\rm gr} = \mu"_{i1} k_{i1} \Delta C_i^L = \frac{\Delta C_{i0}^L + \dfrac{v_T \delta t}{k_{i1}}}{1 + \dfrac{\gamma_0^S M_i g_i}{M_0 m_{k0}^L} \dfrac{C_{k0}^L}{C_k^S} \left(C_i^S - C_{i0}^L \right) \mu"_{i1} k_{i1} \delta t} \mu"_{i1} k_{i1}. \tag{39}$$

Relation $v_{\rm gr} - v_T$ is obviously linear (Figure 4).

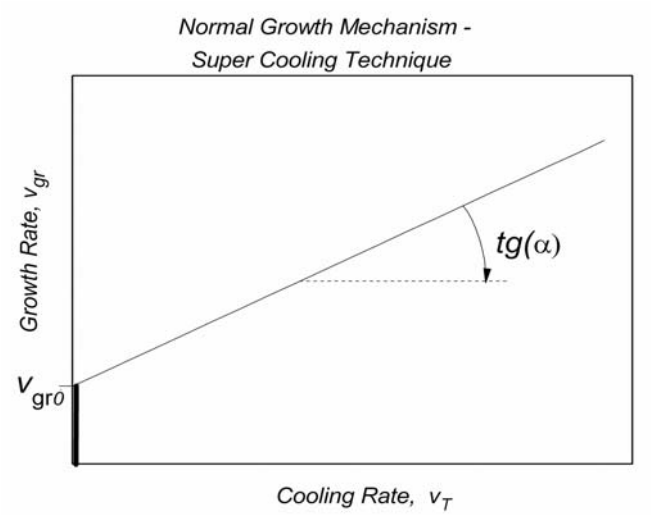

Figure 4. Growth rate $v_{\rm gr}$ versus cooling rate v_T in the case of normal growth mechanism by supercooling technique .

Last equation allows the determination of the initial growth rate $v_{\rm gr0}$ at $v_T \to 0$ and the slope of the curve: $dv_{\rm gr}/dv_T = \tan\alpha$.

$$\tan\alpha = \frac{\mu"_{i1} \delta t}{1 + \dfrac{\gamma_0^S M_i g_i}{M_0 m_{k0}^L} \dfrac{C_{k0}^L}{C_k^S} \left(C_i^S - C_{i0}^L \right) \mu"_{i1} k_{i1} \delta t} = \frac{M_0 \tilde{m}_{kn-1}^L}{\gamma_0^S M_i g_i k_{in}} \frac{C_k^S}{\tilde{C}_{kn-1}^L \left(C_i^S - \tilde{C}_{in-1}^L \right)}. \tag{40}$$

$$v_{\mathrm{gr0}} = \frac{\mu"_{i1} k_{i1} \Delta C_{i0}^{L}}{1 + \dfrac{\gamma_0^S M_i g_i}{M_0 m_{k0}^L} \dfrac{C_{k0}^L}{C_k^S} \left(C_i^S - C_{i0}^L \right) \mu"_{i1} k_{i1} \delta t}. \tag{41}$$

At small values of the cooling rate, the growth rate is determined by the initial supersaturation ΔC_{i0}^L, as expected. The quantities ΔC_{i0}^L and δt are as a rule well known, the ratio $v_{\mathrm{gr0}}/\tan\alpha$ provides the slope of the liquidus surface k_{i1} with respect to the i-component: $v_{\mathrm{gr0}}/\tan\alpha = k_{i1}\Delta C_{i0}^L/\delta t$.

In the case of normal mechanism of growth realized by equilibrium cooling technique the relation $v_{\mathrm{gr}}(v_T)$ is linear again (Figure 5). Substituting equation (20) into (7), one obtains the relation between the growth rate and the cooling rate:

$$v_{\mathrm{gr}} = \mu"_{i1} k_{i1} \Delta C_{i1}^L = \frac{\mu"_{i1} v_T \delta t}{1 + \dfrac{\gamma_0^S M_i g_i}{M_0 m_{k0}^L} \dfrac{C_{k0}^L}{C_k^S} \left(C_i^S - C_{i0}^L \right) \mu"_{i1} k_{i1} \delta t}. \tag{42}$$

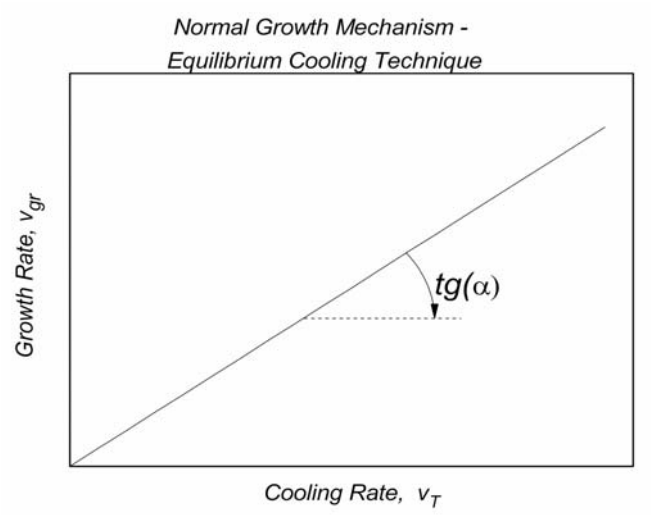

Figure 5. The effect of the cooling rate v_T on the growth rate v_{gr} in case of normal growth mechanism by equilibrium cooling technique.

The function $v_{\mathrm{gr}}(v_T)$ in the coordinates $v_{\mathrm{gr}} - v_T$ is linear. The point $(v_{\mathrm{gr}} = v_T = 0)$ belongs to the function, because no initial supersaturation is available. Equation (42) may be derived from equation (39) at $\Delta C_{i0}^L = 0$. The slope of the line $dv_{\mathrm{gr}}/dv_T = \tan\alpha$ from Figure 5, obtained from equation (42), is the same as the slope of the line from equation (40).

In the case of screw dislocations growth mechanism the situation is substantially different. For the supercooling technique, from equations (12) and (10) one obtains the relation $v_{\mathrm{gr}}(v_T)$. In general, it has the form:

$$v_{\mathrm{gr1}} = \mu_{i1} k_{i1}^2 {\Delta C_{i1}^L}^2 = A^{(1)} + B^{(1)} v_T - \sqrt{{C^{(1)}}^2 + D^{(1)} v_T}. \tag{43}$$

At $v_T{}^* = [(D^{(1)}/2B^{(1)})^2 - C^{(1)2}]/D^{(1)} = -k_{i1}\Delta C^L_{i0}/\delta t$ there is a minimum (Figure 6). This minimum is devoid of sense, because a negative value of the cooling rate $v_T{}^*$ is impossible - in an epitaxial process it would mean that no cooling but a heating takes place.

In this case the function $v_{\rm gr}(v_T)$ is parabolic at low values of the cooling rate. At high values of the cooling rate the function $v_{\rm gr}(v_T)$ is linear. Using equation (43), one may obtain the parameters $v_{\rm gr0}$, α_1 and α_2, shown in Figure 6.

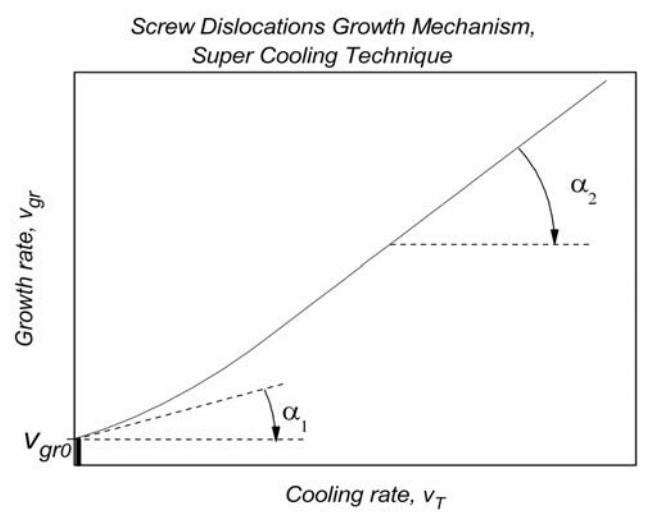

Figure 6. Growth rate versus cooling rate for the case of screw dislocations growth mechanism using the supercooling technique.

$$
\begin{aligned}
v_{\rm gr0} &= A^{(1)} - C^{(1)} = \frac{\mu_{i1}k_{i1}^2}{2H_{i1}^2}\left[\left(1+2H_{i1}\Delta C^L_{i0}\right) - \left(1+4H_{i1}\Delta C^L_{i0}\right)^{1/2}\right],\\
(dv_{gr}/dv_T)_{v_T\to\infty} &= \tan\alpha_2 = B^{(1)} = \frac{\mu_{i1}k_{i1}\delta t}{H_{i1}},\\
(dv_{gr}/dv_T)_{v_T\to 0} &= \tan\alpha_1 = B^{(1)} - \frac{D^{(1)}}{2\sqrt{C^{(1)}}} = \frac{[(\Delta_{i1}-1)/\Delta_{i1}]\,\mu_{i1}k_{i1}\delta t}{H_{i1}},
\end{aligned}
\tag{44}
$$

where $\Delta_{i1} = \sqrt{1+4H_{i1}\Delta C^L_{i0}}$ and $H_{i1} = \frac{\gamma_0^S M_i g_i}{M_0 m^L_{k0}}\frac{C^L_{k0}}{C^S_k}\left(C^S_i - C^L_{i0}\right)\mu_{i1}k_{i1}^2\delta t$ (equation (12)). The initial growth rate $v_{\rm gr0}$ depends on the initial supersaturation ΔC^L_{i0} reasonably. By the quantities C^L_{i0}, C^L_{k0} and m^L_{k0} it depends also on the process temperature and on the slope of the liquidus surface k_i in respect to the i-component. By the kinetic coefficient μ_i the initial growth rate $v_{\rm gr0}$ depends on the process of ad-atoms surface migration.

An analogous situation arises in the case of equilibrium cooling technique. By substituting the supersaturation ΔC^L_{i1} from equation (23) into equation (10) one obtains the relation $v_{\rm gr}(v_T)$ for the case of equilibrium cooling technique and screw dislocations growth mechanism.

$$
v_{\rm gr1} = \mu_{i1}k_{i1}^2{\Delta C^L_{i1}}^2 = A^{(0)} + B^{(0)}v_T - \sqrt{{A^{(0)}}^2 + D^{(0)}v_T}. \tag{45}
$$

It is again a parabolic relation with minimum at $v_{\rm gr} = v_T = 0$ (Figure 7). The parabolic relation is observed at low values of the cooling rate ($v_T \to 0$). At high values of the cooling rate this dependence is linear again. Using equation (45), the slope of the curve at large values of the cooling rate one may determine:

$$\tan\alpha = (dv_{\rm gr}/dv_T) \approx B^{(0)} = \frac{\mu_{i1} k_{i1} \delta t}{H_{i1}}. \tag{46}$$

The last relation is the same as in the case shown on Figure 6 (eq. (44)): $dv_{\rm gr}/dv_T = \tan\alpha_2$.

Relation $v_{\rm gr}(v_T)$ in the case of two-dimensional nuclei growth is unknown, because the problem is solved graphically. Because of that, this growth mechanism can not be revealed clearly (in an analytical form).

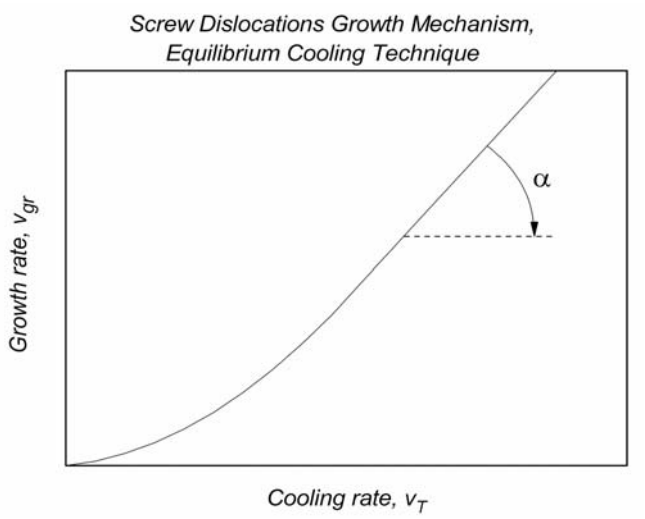

Figure 7. Relation $v_{\rm gr}(v_T)$ in the case of screw dislocations mechanism of growth using equilibrium cooling technique.

Relation $v_{\rm gr}(v_T)$ may be established experimentally. In all the experiments the initial temperature T_0, the area of the grown layer, the thickness of the liquid phase above the substrate, the duration of the process δt, must remain constant. The cooling rate only must be changed in these experiments. Of special importance in these experiments is the region of low values of the cooling rate: $v_T \to 0$. This way only, one may establish the availability of a parabolic relation between the growth rate and the cooling rate.

In previous work [34] it has been demonstrated the possibility of determining the crystallization mechanism in an LPE process by the relation $v_{\rm gr} - \Delta C_{i0}^L$. In the case of screw dislocations growth mechanism this relation provides a sigmoidal form, while in the case of normal growth mechanism it is linear. Hence, using the relation $v_{\rm gr}(\Delta C_{i0}^L)$ one may determine the crystal growth mechanism in all the cases in which the crystal growth starts by an initial supersaturation ($\Delta C_{i0}^L \neq 0$) - these are the step cooling technique and the supercooling technique. By the equilibrium cooling technique this approach is not usable ($\Delta C_{i0}^L = 0$).

The present work has demonstrated the possibility of determining the crystallization mechanism by the relation $v_{\rm gr}(v_T)$. In the case of screw dislocation growth this relation is parabolic at low values of the cooling rate. In the case of normal growth, it is linear. Therefore, this approach allows the determination of the crystallization mechanism in all the cases in which the crystal growth is caused by temperature cooling ($v_T \neq 0$) - these are the supercooling technique and the equilibrium cooling technique. This approach is not usable in the case of step cooling technique ($v_T = 0$).

6. Conclusion

The objective of the present work was to discuss the possibility of determining the crystallization mechanisms in the case of all the three liquid phase epitaxy techniques, used in the practice - the step cooling technique, the supercooling technique and the equilibrium cooling technique. For these purposes the transient growth process has been investigated. It has been shown that the use of the relation $v_{\rm gr}(v_T)$ allows one to determine the crystallization mechanism and make clear distinction between the two crystal growth mechanisms - the normal growth and by the screw dislocations assisted growth. In the case of linear relation between the growth rate $v_{\rm gr}$ and the cooling rate v_T, a normal growth mechanism takes place. If this relation is parabolic, a screw dislocations growth mechanism is involved. One must point out that this parabolic relation may be observed only at low cooling rates - at large values of the cooling rate the relation $v_{\rm gr}(v_T)$ is linear again. By this approach one may not reveal the two-dimensional nuclei growth mechanism - the equations obtained here can not be solved analytically but graphically, which hinders one to reveal the relation $v_{\rm gr}(v_T)$ in an analytical form. It is worth to be pointed out that the supersaturation above the phase boundary increases with increasing cooling rate - equations (9), (12), (22) and (25). Large values of the supersaturation may cause the occurrence of three-dimensional nuclei in the volume of the liquid phase. These nuclei will substantially reduce the growth rate of the epitaxial layer on the substrate, and herewith the shape of the curve $v_{\rm gr}(v_T)$ may prove to be different.

References

[1] A. Rameix, C. Bore1, B. Chambaz, B. Ferrand, D. P. Shepherd, T. J. Warburton, D. C. Hanna, A. C. Tropper, Opt. Commun., **142**, 239 (1997).

[2] A. Erb, E. Walker, R. Fluekiger, Physica C, **245**, 245 (1995).

[3] Y. Yamada and Y. Shiohara, Physica C, **217**, 182 (1993).

[4] Xin Yao, Teruo Izumi, Yuh Shiohara, Physica C, **386**, 374 (2003).

[5] B. Ferrand, D. Pelenc, I. Chartier and Ch. Wyon, J. Cryst. Gr. **128**, 966 (1993).

[6] D. Pelenc, Chambaz, I. Chartier, B. Ferrand, C. Wyon, D. P. Shepherd, D. C. Hanna, A. C. Large, A. C. Tropper, Opt. Commun., **115**, 491 (1995).

[7] K. Kakimoto, Y. Sugawara, T. Izumi, Y. Shiohara, Physica C, **334**, 249 (2000).

[8] Hitoshi Tamada, Atsuo Yamada, and Masaki Saitoh, J. Appl. Phys., **70**, 2536 (1991).

[9] T. Kawaguchi, M. Imaeda, R. Ohuchi, M. Minakata, T. Taniuchi, T. Fukuda, J. Cryst. Gr., **166**, 493 (1996).

[10] P. Rogin, J. Hulliger, J. Cryst. Gr., **179**, 551 (1997).

[11] Atsushi Takagi, Jian-Guo Wen, Izumi Hirabayashi, Uichiro Mizutani, J. Cryst. Gr., **193**, 71 (1998).

[12] Tatsuo Kawaguchi, Dae-Ho Yoon, Makoto Minakata, Yasumasa Okada, Minoru Imaeda, Tsuguo Fukuda, J. Cryst. Gr., **152**, 87 (1995).

[13] Y. Yamada and Y. Shiohara, Physica C, **217**, 182 (1993).

[14] Ruixing Liang, P. Dosanjh, D. A. Bonn, D. J. Baar, J. F. Carolan and W. N. Hardy, Physica C, **195**, 51 (1992).

[15] P. Benema, J. Cryst. Gr., **24/25**, 1, 76 (1974).

[16] V. M. Andreev et. al., Techn. Phys. Lett., **14**, 15, 1429 (1989).

[17] J. I. Alferov et. al., Techn. Phys. Lett., **14**, 2, 171 (1988).

[18] J. I. Alferov et. al., Techn. Phys. Lett., **14**, 1, 76 (1988).

[19] J. I. Alferov et. al., Techn. Phys. Lett., **14**, 2, 171 (1989).

[20] W. Burton., N. Cabrera, F. Frank, Phil. Trans., A, **243**, 299 (1951).

[21] W. A. Tiller, J. Cryst. Gr., **6**, 77, (1969).

[22] W. Hillig, D. Turnbull, J. Chem. Phys., **24**, 914 (1956).

[23] N. S. Peev, Cryst. Res. Techn., **21**, 1, 319 (1986).

[24] H. Casey, M. Panish, *Heterostructure Lasers*, (Mir, Moskow, 1981 (in Russian)).

[25] J. J. Hsieh, J. Cryst. Gr., **27**, 49 (1974).

[26] V. M. Andreev et. al., *Liquid Phase Epitaxy in the Technology of Semiconductor Devices*, (Sovetskoe Radio, Moscow, 1975).

[27] N. S. Peev, Cryst. Res. Techn., **25**, 6, 653 (1990).

[28] N. S. Peev, Cryst. Res. Techn., **25**, 11, 1265 (1990).

[29] N. S. Peev, Cryst. Res. Techn., **34**, 7, 851 (1999).

[30] N. S. Peev, Comptes rendus de l'Acadmie Bulgare des Sciences, **53**, 5, 43 (2000).

[31] N. S. Peev, J. Res. Phys., **29**, 2, 85, (2003).

[32] N. S. Peev, Dissertation, LETI, Leningrad, (1979).

[33] N. S.Peev, Cryst. Res. Techn., **21**, No. 1, 319-326 (1986).

[34] N. S.Peev, Cryst. Res. Techn., **45**, No. 6, 593-599 (2010).

[35] W. A. Tiller, in Floating Zone Editor I. Vigdorovich, (Metallurgy, Moskow, p. 110, 1966) (in Russian).

Journal of Research in Physics Vol. 34, No. 1, 23 - 32 (2010)

Ground state wave functions of superconductivity on honeycomb lattice

M. V. Milovanović
Scientific Computing Laboratory, Institute of Physics, University of Belgrade, P. O. Box 68, 11 000 Belgrade, Serbia

Received: *November 22, 2010*

Abstract

We derive ground state wave functions of superconducting instabilities on the honeycomb lattice induced by nearest-neighbor attractive interactions. They reflect the Dirac nature of electrons in the low-energy limit. For the order parameter that is the same irrespective of the direction to any of the nearest neighbors we find weak pairing (slowly decaying) behavior in the orbital part of the Cooper pair with no angular dependence. At the neutrality point, in the spin-singlet case, we recover a strong pairing behavior.

1. Introduction

The advent of graphene [1] opened a door for exploration of new phenomena in two-dimensional Dirac-like condensed matter systems. One of the intriguing questions is concerned with superconducting correlations of electrons on the honeycomb lattice system. Superconductivity has been induced in short graphene samples through proximity effect with superconducting contacts [2]. This indicates that Cooper pairs can propagate coherently in th graphene. In principle, superconductivity on the graphene honeycomb lattice can be induced by short-range attractive interactions and explorations of allowed possibilities were given in [3, 4, 5]. Among the most interesting is the so-called $p + ip$ superconducting instability introduced in [3]. It is supported by the most natural nearest-neighbor attractive interaction and have distinct features of the Dirac electrons. Later, it has been shown [5], by a restricted (low-energy) analysis, that this state may be less energetically favorable with respect to Kekule-like order parameter arrangements. Nevertheless, the $p + ip$ instability seems, though an exotic state, a very attractive possibility because of its underlying symmetry of the order parameter, the same as for Pfaffian quantum Hall state [6] or $p+ip$ spinless superconductor [7]. The latter systems support non-Abelian statistics, which is at the heart of the idea of the topological computing [8]. There is an important difference between these states and the proposed graphene state. The superconducting instability in graphene does not break time-reversal symmetry and those systems do. Due to the valley degeneracy we effectively have two $(p \pm ip)$ order parameters and this requires additional understanding of intertwined correlations and underlying symmetries. One way, just as in the Pfaffian state [7], is to look for the ground state wave function and recognize the structures and symmetries.

In this paper we derive an effective (long-distance) expression for the ground state wave function of the $p+ip$ spin-singlet instability described in Ref. 3 and display the pertinent symmetries in this case. Also, a spinless case will be discussed. We will use the BCS mean-field formalism. In the following section we will set up the BCS formalism, solve the Bogoliubov - de Gennes (BdG) equations and find the expression for the ground state wave functions. The last section is devoted to conclusions.

2. Superconductivity on honeycomb lattice and its ground states

The Hamiltonian for free electrons on the honeycomb lattice is

$$H_0 = -t\sum_{\langle ij\rangle}\sum_{\sigma=\uparrow,\downarrow}(a^\dagger_{i,\sigma}b_{j,\sigma}+h.c.) - \mu\sum_i \hat{n}_i, \tag{1}$$

where t is the hopping energy between nearest neighbor C (carbon) atoms, $a_{i,\sigma}(a^\dagger_{i,\sigma})$ is the on-site annihilation (creation) operator for electrons in the sublattice A with spin $\sigma=\uparrow,\downarrow$, and $b_{i,\sigma}(b^\dagger_{i,\sigma})$ for sublattice B, $\hat{n}_i$ is the on-site number operator, and μ is the graphene chemical potential. We use units such that $\hbar=1$. Diagonalization of Eq.(1) leads to a spectrum given by: $\epsilon_{\vec{k}}=\pm t|S(\vec{k})|$, where $\vec{k}$ is the two-dimensional momentum, and $S(\vec{k})=\sum_{\vec{\delta}}\exp\{i\vec{k}\vec{\delta}\}$ with $\vec{\delta}$'s defined as $\delta_1=a(0,1/\sqrt{3})$, $\delta_2=a/2(1,-1/\sqrt{3})$, and $\delta_3=a/2(-1,-1/\sqrt{3})$, and $a=\sqrt{3}\ a_{cc}$, a_{cc} is the distance between C atoms and a is the next to nearest neighbor distance. At the corners of the hexagonal Brillouin zone, $\vec{K}_\pm=(2\pi)/a(2/3,0)$, we have $S(\vec{K}_\pm+\vec{k})\approx\mp a\sqrt{3}/2(k_x\mp ik_y)$, and the band has the shape of a Dirac cone: $\epsilon(\vec{K}_\pm+\vec{k})=\pm v_F|\vec{k}|$, where $v_F=(\sqrt{3}at)/2$ is the Fermi-Dirac velocity.

For the sake of simplicity we will consider only nearest-neighbor attractive interactions among electrons. The on-site repulsive interactions can be introduced and will not change our conclusions. Therefore the complete Hamiltonian will include nearest-neighbor interactions as follows,

$$H_I = g\sum_{\langle ij\rangle}\sum_{\sigma,\sigma'}a^\dagger_{i,\sigma}a_{i,\sigma}b^\dagger_{j,\sigma'}b_{j,\sigma'}, \tag{2}$$

where $g<0$. We will assume the spin-singlet pairing among nearest-neighbors and apply the BCS ansatz with $\Delta_{ij}=\langle a_{i,\downarrow}b_{j,\uparrow}-a_{i,\uparrow}b_{j,\downarrow}\rangle$, the superconducting order parameter. Furthermore we assume one and the same $\Delta_{ij}=\Delta$ for all nearest neighbors, which, due to global gauge ($U(1)$) transformations on a's and b's, can be chosen real and positive. The interaction part, H_I, becomes

$$\tilde{H}_{BCS} = \{g\sum_{\langle ij\rangle}\Delta(a^\dagger_{i,\uparrow}b^\dagger_{j,\downarrow}-a^\dagger_{i,\downarrow}b^\dagger_{j,\uparrow})+h.c.\}-3g|\Delta|^2. \tag{3}$$

The order parameter in the momentum space is

$$\Delta_{\vec{k}}=\sum_{\langle ij\rangle}\Delta\exp\{i\vec{k}(\vec{i}-\vec{j})\}=\Delta\sum_{\vec{\delta}}\exp\{i\vec{k}\vec{\delta}\}=\Delta S(\vec{k}). \tag{4}$$

Therefore near K points $\Delta_{\vec{K}_\pm+\vec{k}}\sim\mp(k_x\mp ik_y)$, which then describes two p-wave like superconducting order parameters in a low effective description. The complete BCS Hamiltonian can be now cast in the following form in the momentum space,

$$H_{BCS} = \sum_{\vec{k}} \phi^{\dagger}_{\vec{k}} M_{\vec{k}} \phi_{\vec{k}}, \tag{5}$$

where

$$\phi^{\dagger}_{\vec{k}} = (a^{\dagger}_{\vec{k}\uparrow}, b^{\dagger}_{\vec{k}\uparrow} a_{-\vec{k}\downarrow}, b_{-\vec{k}\downarrow}), \tag{6}$$

with defined $a_{\vec{k}\sigma} = \sum_i a_{i\sigma} \exp\{i\vec{k}\ \vec{i}\}$ and $b_{\vec{k}\sigma} = \sum_i b_{i\sigma} \exp\{i\vec{k}\ \vec{i}\}$, and, with $g\Delta \equiv \Delta$ for short,

$$M_{\vec{k}} = \begin{bmatrix} -\mu & -tS(\vec{k}) & 0 & \Delta S(\vec{k}) \\ -tS^*(\vec{k}) & -\mu & \Delta S(-\vec{k}) & 0 \\ 0 & \Delta S^*(-\vec{k}) & \mu & tS(\vec{k}) \\ \Delta S^*(\vec{k}) & 0 & tS^*(\vec{k}) & \mu \end{bmatrix}.$$

We look for the solution in the form of a diagonalized Bogoliubov BCS Hamiltonian,

$$H_{BCS} = \sum_{\vec{k},\gamma=\pm} \omega^{\alpha}_{\vec{k},\gamma} \alpha^{\dagger}_{\vec{k},\gamma} \alpha_{\vec{k},\gamma} + \sum_{\vec{k},\gamma=\pm} \omega^{\beta}_{\vec{k},\gamma} \beta^{\dagger}_{\vec{k},\gamma} \beta_{\vec{k},\gamma} + E_0, \tag{7}$$

where $\alpha_{\vec{k},\gamma}$ and $\beta_{\vec{k},\gamma}$, $\gamma = \pm$ are new quasiparticles at momentum $\vec{k}$. For the dispersions we have:

$$\omega^{\alpha}_{\vec{k},\gamma} = \gamma\omega^{\alpha}_{\vec{k}} \quad \text{and} \quad \omega^{\beta}_{\vec{\mathrm{k}},\gamma} = \gamma\omega^{\beta}_{\vec{\mathrm{k}}}, \tag{8}$$

where $\gamma = \pm$. We define a general solution α as

$$\alpha_{\vec{k}} = u_{\vec{k},\uparrow} a_{\vec{k},\uparrow} + v_{\vec{k},\uparrow} b_{\vec{k},\uparrow} + u_{\vec{k},\downarrow} a^{\dagger}_{-\vec{k},\downarrow} + v_{\vec{k},\downarrow} b^{\dagger}_{-\vec{k},\downarrow}. \tag{9}$$

Next we have to solve the Bogoliubov - de Gennes (BdG) equations, which follow from the following condition,

$$[\alpha_{\vec{k}}, H_{BCS}] = E\alpha_{\vec{k}}. \tag{10}$$

From this matrix eigenvalue problem we obtain energies of the Bogoliubov quasiparticles,

$$\omega^{p}_{\vec{k}} = \pm\sqrt{(v_F|S(\vec{k})| + p\mu)^2 + |\Delta S(\vec{k})|^2}, \tag{11}$$

where $\pm$ stands for the particle and hole branches respectively for two kinds of excitations $p = -1(\alpha)$ and $p = +1(\beta)$. For $\mu = 0$ the system is gapless and we need a coupling g larger than a critical value for the superconducting instability to exist [3]. This can be found considering in the BCS formalism the consistency or gap equation.

For each valley we have to solve the Bogoliubov problem using the expansion $S(\vec{K}_{\pm} + \vec{k}) \approx \mp a\sqrt{3}/2(k_x \mp ik_y)$. Near K_+ we need to diagonalize the following matrix, $M^*_{\vec{k}}$, that comes out from Eq. (10):

$$\begin{bmatrix} -\mu & v_F k & 0 & sk \\ v_F k^* & -\mu & sk^* & 0 \\ 0 & sk & \mu & -v_F k \\ sk^* & 0 & -v_F k^* & \mu \end{bmatrix},$$

where $s = s^* = -\Delta a\sqrt{3}/2 > 0$. Its eigenvectors (after normalization) enter the following expressions for Bogoliubov quasiparticles:

$$\begin{aligned} \alpha_{\vec{k},+} &= \frac{1}{2\sqrt{E_\alpha[E_\alpha - (\mu - v_F|k|)]}}\{[E_\alpha - (\mu - v_F k)](\sqrt{\frac{k}{k^*}}a_{+\uparrow} + b_{+\uparrow}) + \\ &+ s|k|(\sqrt{\frac{k}{k^*}}a^\dagger_{-\downarrow} + b^\dagger_{-\downarrow})\}, \end{aligned} \tag{12}$$

and

$$\begin{aligned} \beta_{\vec{k},+} &= \frac{1}{2\sqrt{E_\beta[E_\beta - (\mu + v_F|k|)]}}\{[E_\beta - (\mu + v_F k)](\sqrt{\frac{k}{k^*}}a_{+\uparrow} - b_{+\uparrow}) - \\ &- s|k|(\sqrt{\frac{k}{k^*}}a^\dagger_{-\downarrow} - b^\dagger_{-\downarrow})\}, \end{aligned} \tag{13}$$

and quasiholes:

$$\begin{aligned} \alpha_{\vec{k},-} &= \frac{1}{2\sqrt{E_\alpha[E_\alpha + (\mu - v_F|k|)]}}\{-[E_\alpha + (\mu - v_F k)](\sqrt{\frac{k}{k^*}}a_{+\uparrow} + b_{+\uparrow}) + \\ &+ s|k|(\sqrt{\frac{k}{k^*}}a^\dagger_{-\downarrow} + b^\dagger_{-\downarrow})\}, \end{aligned} \tag{14}$$

and

$$\begin{aligned} \beta_{\vec{k},-} &= \frac{1}{2\sqrt{E_\beta[E_\beta + (\mu + v_F|k|)]}}\{-[E_\beta + (\mu + v_F k)](\sqrt{\frac{k}{k^*}}a_{+\uparrow} - b_{+\uparrow}) - \\ &- s|k|(\sqrt{\frac{k}{k^*}}a^\dagger_{-\downarrow} - b^\dagger_{-\downarrow})\}, \end{aligned} \tag{15}$$

for the Bogoliubov solution near point $\vec{K}_+$, where we denoted $a_{\vec{K}_\pm \pm \vec{k},\sigma} \equiv a_{\pm\sigma}$ and $b_{\vec{K}_\pm \pm \vec{k},\sigma} \equiv b_{\pm\sigma}$.

The natural eigenstates of chirality appeared in our expressions. For example, $(\sqrt{\frac{k}{k^*}}a_{+\uparrow} + b_{+\uparrow})$ represents the spinor:

$$\chi = \begin{bmatrix} \sqrt{\frac{k^*}{k}} \\ 1 \end{bmatrix}, \tag{16}$$

which is the eigenstate of the chirality operator $\frac{\vec{\sigma}\vec{k}}{|k|}$, defined with $\vec{\sigma} = (\sigma_x, \sigma_y)$ Pauli matrices, i.e. the pseudospin (due to two sublattices) is along the momentum vector. The state $(\sqrt{\frac{k^*}{k}}a_{-\downarrow} + b_{-\downarrow})$ represents the same spinor because of the interchanged roles of sublattices

at the $\vec{K}_-$ point. To see this in more detail we would like to remind the reader that instead of the Dirac free electron representation by the spinor

$$\chi^\dagger_{\vec{k}} = (a^\dagger_{\vec{K}_+ + \vec{k},\sigma}, b^\dagger_{\vec{K}_+ + \vec{k},\sigma} b^\dagger_{\vec{K}_- + \vec{k},\sigma}, a^\dagger_{\vec{K}_- + \vec{k},\sigma}), \tag{17}$$

and the chirality operator defined as

$$\begin{bmatrix} \frac{\vec{\sigma}\vec{k}}{|\vec{k}|} & 0 \\ 0 & -\frac{\vec{\sigma}\vec{k}}{|\vec{k}|} \end{bmatrix}, \tag{18}$$

in the BdG formalism we work with

$$\begin{aligned} \phi^\dagger_{\vec{k}} &= (a^\dagger_{\vec{K}_+ + \vec{k}\uparrow}, b^\dagger_{\vec{K}_+ + \vec{k}\uparrow} a_{\vec{K}_- - \vec{k}\downarrow}, b_{\vec{K}_- - \vec{k}\downarrow}) \\ &\equiv (a^\dagger_{+\uparrow}, b^\dagger_{+\uparrow} a_{-\downarrow}, b_{-\downarrow}). \end{aligned} \tag{19}$$

Note the reversed order of sublattices and the change of the sign of the momentum $\vec{k}$ near $\vec{K}_-$ point in the BdG formalism with respect to the free one. Thus, the lower 2×2 matrix on the diagonal of the Hamiltonian matrix in the free Dirac case can be read off from:

$$\begin{bmatrix} b^\dagger_{\vec{K}_- + \vec{k},\sigma} & a^\dagger_{\vec{K}_- + \vec{k},\sigma} \end{bmatrix} \begin{bmatrix} -\mu & -v_F k^* \\ -v_F k & -\mu \end{bmatrix} \begin{bmatrix} b_{\vec{K}_- + \vec{k},\sigma} \\ a_{\vec{K}_- + \vec{k},\sigma} \end{bmatrix}, \tag{20}$$

i.e. it is equal to $-v_F \vec{k}\vec{\sigma} - \mu$. Note that if we change the sign of $\vec{k}$ vector in Eq.(20) i.e. $\vec{k} \to -\vec{k}$ the off-diagonal elements in the matrix will change the sign, so that in this basis in the free representation the chirality operator will not have minus sign in the lower right entry of the matrix representation in Eq.(18). Therefore, $(\sqrt{\frac{k^*}{k}} a_{-\downarrow} + b_{-\downarrow})$ represents the same spinor (up to a phase factor) as in Eq.(16) and the same chirality eigenstate (with positive eigenvalue) as we pointed out earlier. Nevertheless, in the Bogoliubov representation we still have

$$\begin{bmatrix} a_{-\downarrow} & b_{-\downarrow} \end{bmatrix} \begin{bmatrix} \mu & -v_F k^* \\ -v_F k & \mu \end{bmatrix} \begin{bmatrix} a^+_{-\downarrow} \\ b^+_{-\downarrow} \end{bmatrix}, \tag{21}$$

i.e. the matrix is $-v_F \vec{k}\vec{\sigma} + \mu$, and the representation of the chirality operator remains the same as in Eq.(18). We will use this fact later on. On the other hand, the combinations in Eqs. (13) and (15): $(\sqrt{\frac{k}{k^*}} a_{+\uparrow} - b_{+\uparrow})$ and $(\sqrt{\frac{k^*}{k}} a_{-\downarrow} - b_{-\downarrow})$ have the pseudospin vector in the opposite direction of the momentum vector $\vec{k}$.

It is thus natural to introduce the following notation:

$$\sqrt{\frac{k}{k^*}} a_{+\uparrow} + b_{+\uparrow} \equiv c_{+\uparrow v}, \tag{22}$$

$$\sqrt{\frac{k}{k^*}} a^\dagger_{-\downarrow} + b^\dagger_{-\downarrow} \equiv c^\dagger_{-\downarrow v}, \tag{23}$$

$$\sqrt{\frac{k}{k^*}} a_{+\uparrow} - b_{+\uparrow} \equiv c_{+\uparrow w}, \tag{24}$$

$$-\sqrt{\frac{k}{k^*}}a^\dagger_{-\downarrow} + b^\dagger_{-\downarrow} \equiv c^\dagger_{-\downarrow w}, \tag{25}$$

where v and w denote the chirality, i.e. whether the pseudospin vector is along or in the opposite direction with respect to the $\vec{k}$ vector, respectively. We have to note that these electron operators are defined up to a phase factor, most importantly, the $\sqrt{\frac{k}{k^*}}$ phase. This degree of freedom should not influence the physics, but we chose the definitions so that the symmetry under exchange of particles in the ground state wave function is transparent.

The α and β sectors are obviously decoupled in the Bogoliubov description, and we can concentrate on and examine closely the α sector first. Furthermore, we do not have to consider $\vec{K}_-$ point separately as the symmetry considerations tell us that the BdG equations around this point will induce the coupling or states of an electron around $\vec{K}_+$ point with $\downarrow$ projection of spin and those around $\vec{K}_-$ point with $\uparrow$ projection of spin.

Thus it suffices to consider the α sector first (with $c_{+\uparrow v}$ and $c_{-\downarrow v}$) and then use the symmetry arguments, more precisely antisymmetry under real spin exchange, to recover the whole ground state wave function. We can rewrite α's in the following form,

$$\alpha_{k,+} = u^p_k c_{+\uparrow v} + v^p_k c^\dagger_{-\downarrow v}, \tag{26}$$

$$\alpha_{k,-} = u^h_k c_{+\uparrow v} + v^h_k c^\dagger_{-\downarrow v}. \tag{27}$$

We should demand $\alpha_{k,+}|G\rangle = 0$ and $\alpha^\dagger_{k,-}|G\rangle = 0$, for any k, if $|G\rangle$ is to represent the ground state vector. That implies that in the α sector of $\vec{K}_+$ point we have the following contribution to the ground state,

$$\prod_k (u^p_k - v^p_k c^\dagger_{+\uparrow v} c^\dagger_{-\downarrow v})|0\rangle, \tag{28}$$

where $|0\rangle$ denotes the vacuum. This state is annihilated with both, $\alpha_{k,+}$ and $\alpha^\dagger_{k,-}$. The symmetry arguments demand that we should get a similar expression considering the BdG equations at $\vec{K}_-$ point. If we denote by $g_\alpha(k) = -\frac{v^p_k}{u^p_k}$, the ground state vector in the α sector should look like:

$$\begin{aligned} &\prod_k (1 + g_\alpha(k) c^\dagger_{+\uparrow v} c^\dagger_{-\downarrow v})(1 + g_\alpha(k) c^\dagger_{-\uparrow v} c^\dagger_{+\downarrow v})|0\rangle = \\ = &\prod_k \{1 + g_\alpha(k)[c^\dagger_{+\uparrow v} c^\dagger_{-\downarrow v} + c^\dagger_{-\uparrow v} c^\dagger_{+\downarrow v}] + \frac{g^2_\alpha(k)}{2}[c^\dagger_{+\uparrow v} c^\dagger_{-\downarrow v} + c^\dagger_{-\uparrow v} c^\dagger_{+\downarrow v}]^2|0\rangle \\ = &\exp\{\sum_k g_\alpha(k)[c^\dagger_{+\uparrow v} c^\dagger_{-\downarrow v} + c^\dagger_{-\uparrow v} c^\dagger_{+\downarrow v}]\}|0\rangle. \end{aligned} \tag{29}$$

Now we can identify $g_\alpha(k)$ to represent a Fourier transform of the wave function of a Cooper pair of electrons, which is a spin-singlet with respect to spin degree of freedom and a triplet state (symmetric under exchange) with respect to the valley ($K_\pm$) degree of freedom. If we defined differently our electron operators, there would be the possibility for $g_\alpha(k)$ to acquire the phase factor $\sqrt{\frac{k}{k^*}}$, which would make the identification of the antisymmetry under exchange harder.

Taking into account the β sector (with the chirality in the opposite direction of the momentum: w) the complete ground state vector is

$$\exp\{\sum_k g_\alpha(k)[c^\dagger_{+\uparrow v}c^\dagger_{-\downarrow v} + c^\dagger_{-\uparrow v}c^\dagger_{+\downarrow v}] + \sum_k g_\beta(k)[c^\dagger_{+\uparrow w}c^\dagger_{-\downarrow w} + c^\dagger_{-\uparrow w}c^\dagger_{+\downarrow w}]\}|0\rangle, \tag{30}$$

where

$$g_\alpha(k) = -\frac{s|k|}{E_\alpha - (\mu - v_F|k|)} \quad \text{and} \quad \mathrm{g_\beta(k)} = -\frac{\mathrm{s|k|}}{\mathrm{E_\alpha - (\mu + v_F|k|)}}. \tag{31}$$

Using the long-distance (low-momentum) expansions for E_α and E_β, for a finite μ,

$$E_{\alpha(\beta)} \approx \mu \mp v_F|k| + \frac{s^2|k|^2}{2\mu}, \tag{32}$$

we find the long-distance behavior of the pair wave function to be

$$\lim_{|\vec{r}|\to\infty} g_\alpha(\vec{r}) = \lim_{|\vec{r}|\to\infty} g_\beta(\vec{r}) \sim \frac{1}{|\vec{r}|}, \tag{33}$$

i.e. we have a case for a weak coupling [7]. As emphasized in Ref. 7, the term weak pairing does not mean also weak coupling; it stands for a phase with an unusual large spread of the Cooper pairs. On the other hand, for $\mu = 0$ we have that $g_\alpha(k)$ and $g_\beta(k)$ are two constants and the Cooper pairs are localized on a short scale $\sim a$ in the graphene system at the neutrality point. Thus for $\mu = 0$ we have a case for a strong pairing.

The ground state vector (wave function) in Eq.(30) displays two kinds of Cooper pairs, each antisymmetric under combined exchange of (a) orbital, (b) valley ($\vec{K}_\pm$), and (c) spin ($\uparrow, \downarrow$) degree of freedom. Two kinds of Cooper pairs stem from the chirality (sublattice) degree of freedom intimately connected with the Dirac-nature of the electron with both, particles and holes. They both, particles (with positive chirality v at $\vec{K}_+$) and holes (with negative chirality w at $\vec{K}_+$), constitute Cooper pairs, which are symmetric under $v \leftrightarrow w, v_F \to -v_F$ transformation.

In the long distance limit we recover the form of the wave function of ordinary s-wave superconductor as given in Ref. 9, though with more, two-component, degrees of freedom. The Cooper pair wave function is antisymmetric under spin exchange and symmetric under exchange of valley ($\vec{K}_\pm$), sublattice (v, w), and orbital degrees of freedom.

Next we will discuss the spin-triplet case, more precisely we will assume that the system is spin-polarized and not consider spin in the following. Therefore, fermions are spinless just like in the Pfaffian case, but they live on the honeycomb lattice. We will assume $\langle a_i b_j\rangle = \Delta$. In this case the Bogoliubov problem in Eq.(5) for the spin-singlet pairing transforms into a similar one with $a_{\vec{k},\sigma} \equiv a_{\vec{k}}$ and $b_{\vec{k},\sigma} \equiv b_{\vec{k}}$, and the matrix $M_{\vec{k}}$ becomes as follows

$$M_{\vec{k}} = \begin{bmatrix} -\mu & -tS(\vec{k}) & 0 & \Delta S(\vec{k}) \\ -tS^*(\vec{k}) & -\mu & -\Delta S(-\vec{k}) & 0 \\ 0 & -\Delta S^*(-\vec{k}) & \mu & tS(\vec{k}) \\ \Delta S^*(\vec{k}) & 0 & tS^*(\vec{k}) & \mu \end{bmatrix}.$$

Around the $\vec{K}_+$ point we have

$$\begin{bmatrix} -\mu & v_F k^* & 0 & sk^* \\ v_F k & -\mu & -sk & 0 \\ 0 & -sk^* & \mu & -v_F k^* \\ sk & 0 & -v_F k & \mu \end{bmatrix},$$

where $s = -\Delta a \frac{\sqrt{3}}{2} > 0$ as before. The problem around the $\vec{K}_-$ point is a copy of the problem around the $\vec{K}_+$ point.

Now the $M_{\vec{k}}$ matrix around $\vec{K}_+$ point cannot be cast, as in the spin-singlet case, in the following form,

$$\begin{bmatrix} v_F \vec{\sigma}\vec{k} - \mu I_2 & s\vec{\sigma}\vec{k} \\ s\vec{\sigma}\vec{k} & -v_F \vec{\sigma}\vec{k} + \mu I_2 \end{bmatrix},$$

where I_2 is the 2×2 identity matrix, which commutes with the chirality matrix (Eq.18). $M_{\vec{k}}$ around $\vec{K}_+$ point can be compactly written as

$$\begin{bmatrix} v_F \vec{\sigma}\vec{k} - \mu I_2 & si\vec{k} \times \vec{\sigma} \\ -si\vec{k} \times \vec{\sigma} & -v_F \vec{\sigma}\vec{k} + \mu I_2 \end{bmatrix},$$

and it does not commute with the chirality operator. The eigenstates of the Bogoliubov problem do not have to be the eigenstates of chirality. We find the following eigenvalues $E_p = \pm\sqrt{\mu^2 + |\vec{k}|^2 s^2 + |\vec{k}|^2 v_F^2 + p\, 2\sqrt{\mu^2 v_F^2 |\vec{k}|^2 + s^2 v_F^2 |\vec{k}|^2}}$, where $p = +1(\alpha)$ and $p = -1(\beta)$ are two branches as before. The associated eigenvectors can be written as sums of fermionic particle eigenstates of chirality only at the low-momentum limit and we list those connected with positive eigenvalues,

$$\alpha_{\vec{k},+} = \frac{1}{\sqrt{2(1 + \frac{|k|^2 s^2}{4\mu^2})}} [\frac{|k|s}{2\mu}(-\sqrt{\frac{k}{k^*}} a_+ + b_+) + (\sqrt{\frac{k}{k^*}} a_-^\dagger + b_-^\dagger)], \tag{34}$$

and

$$\beta_{\vec{k},+} = \frac{1}{\sqrt{2(1 + \frac{|k|^2 s^2}{4\mu^2})}} [-\frac{|k|s}{2\mu}(\sqrt{\frac{k}{k^*}} a_+ + b_+) + (-\sqrt{\frac{k}{k^*}} a_-^\dagger + b_-^\dagger)], \tag{35}$$

and negative eigenvalues,

$$\alpha_{\vec{k},-} = \frac{1}{\sqrt{2(1 + \frac{4\mu^2}{|k|^2 s^2})}} [\frac{2\mu}{|k|s}(\sqrt{\frac{k}{k^*}} a_+ + b_+) + (-\sqrt{\frac{k}{k^*}} a_-^\dagger + b_-^\dagger)], \tag{36}$$

and

$$\beta_{\vec{k},-} = \frac{1}{\sqrt{2(1 + \frac{4\mu^2}{|k|^2 s^2})}} [\frac{2\mu}{|k|s}(\sqrt{\frac{k}{k^*}} a_+ - b_+) + (\sqrt{\frac{k}{k^*}} a_-^\dagger + b_-^\dagger)]. \tag{37}$$

Similarly as before we can define

$$\sqrt{\frac{k}{k^*}}a_+ + b_+ \equiv c_{+v}, \tag{38}$$

$$\sqrt{\frac{k}{k^*}}a_-^\dagger + b_-^\dagger \equiv c_{-v}^\dagger, \tag{39}$$

$$\sqrt{\frac{k}{k^*}}a_+ - b_+ \equiv c_{+w}, \tag{40}$$

$$-\sqrt{\frac{k}{k^*}}a_-^\dagger + b_-^\dagger \equiv c_{-w}^\dagger, \tag{41}$$

and the ground state vector can be cast in the following form,

$$\exp\{\sum_{\vec{k}} \frac{2\mu}{s|k|}(c_{+,v}^\dagger c_{-,w}^\dagger + c_{+,w}^\dagger c_{-,v}^\dagger)\}|0\rangle. \tag{42}$$

In this case, each Cooper pair is antisymmetric under exchange of $\vec{K}_\pm$ points, i.e. valley degree of freedom and symmetric under exchange of sublattices, i.e. chirality ($v \leftrightarrow w$). Depending on our definitions for c's two degrees of freedom can exchange the symmetry properties. We find again the weak pairing ($\sim \frac{1}{r}$) behavior in the orbital part.

6. Conclusion

We derived the ground state wave functions for the superconductivity on the honeycomb lattice induced by nearest-neighbor attractive interactions and with order parameter independent of the direction to any of the nearest neighbors. Although the order parameter in momentum space has the $p \pm ip$ form in a low effective description the Cooper pair wave function behaves as an s-wave (with no angular dependence) and decays as $\sim \frac{1}{r}$. Other (discrete) degrees of freedom combine to make the Cooper pair antisymmetric under exchange. At the point of the transition, $\mu = 0$, in the spin-singlet case, a strong pairing (of the order of lattice spacing) occurs.

References

[1] K. S. Novoselov, A. K. Geim, S. V. Morozov, D. Jiang, Y. Zhang, S. V. Dubonos, I. V. Georgieva, and A. A. Firsov, Science **306**, 666 (2004).

[2] H. B. Heersche, P. Jarillo-Herrero, J. B. Oostinga, L. M. K. Vandersypen, and A. F. Morpurgo, Nature **446**, 56 (2007).

[3] B. Uchoa and A. H. Castro Neto, Phys. Rev. Lett. **98**, 146801 (2007).

[4] A. M. Black-Schaffer and S. Doniach, Phys. Rev. B **75** 134512 (2007).

[5] B. Roy and I. Herbut, Phys. Rev. B **82**, 035429 (2010).

[6] G. Moore and N. Read, Nucl.Phys. B **360**, 362 (1991).

[7] N. Read and D. Green, Phys. Rev. B **61**, 10267 (2000).

[8] C. Nayak, S. H. Simon, A. Stern, M. Freedman, and S. Das Sarma, Rev. Mod. Phys. **80**, 1083 (2008).

[9] J. R. Schrieffer, *Theory of Superconductivity*, p. 42, (Addison-Wesley, 1988).

Journal of Research in Physics Vol. 34, No. 1, 33 - 38 (2010)

Stark Shift Measurements for Some Kr III UV Lines

M. Ćirišan[1], R. J. Peláez[2], S. Djurović[1], J. A. Aparicio[2] and S. Mar[2]
[1]*Faculty of Sciences, Department of Physics,*
Trg Dositeja Obradovica 4, 21000 Novi Sad, Serbia
[2]*Departamento de Física Teórica, Atómica y Óptica, Universidad de Valladolid,*
P. Prado de la Magdalena s/n, 47071 Valladolid, Spain

Received: *December 3, 2010*

Abstract

In this work we report new Stark shift data of several doubly ionized krypton lines from UV region (253 nm - 300 nm). A low-pressure arc with a mixture of 8% of krypton and 92% of helium was used as a plasma source. The obtained results are compared with simplified modified semi-empirical calculations.

Key words: Spectral line, Stark shift

1. Introduction

Investigation of ionized krypton spectra is of interest for many reasons. Generally, spectra of inert gases are important for different physics areas, like laser physics, fusion plasma diagnostics, photoelectron spectroscopy, collision physics, astrophysics, etc. Krypton plays an important role in applications like, for example, the development of the spectral lamps [1], developing of lasers and laser techniques [2]. Furthermore, there is an interest in spectroscopic and atomic data of krypton ions. Stark shifts and width of the spectral lines are usually employed for plasma diagnostic purposes, as well as for testing the theoretical calculations. In addition, Stark parameters data of Kr III lines can be useful for the investigation and verification of the regularities and systematic trends [3] in case of doubly ionized noble gases.

In this work, we report 10 measured Stark shifts of UV Kr III spectral lines, all of them being low intensity lines. This is an extension of our work on doubly ionized krypton line Stark parameters [4]. The measurements are performed in a low pressure pulsed arc plasma under the following plasma conditions: electron density $(0.7-2.0) \times 10^{23}$ m^{-3} and electron temperature $(16000 - 22000)$ K.

For determining the Stark shifts, special attention was paid to both experimental and data treatment procedures. Other broadening mechanisms were taken into account, as well.

The present data are new in the literature, and they make a contribution to the existing database of measured Kr III Stark shifts. Up to now, only two papers reported the Kr III Stark shift data [5, 6]. In Di Rocco et al. [5] plasma diagnostics data are missing. On the

other hand, in Milosavljevic et al. [6], all observed spectral lines were above 300 nm. The conclusion is that there are no corresponding experimental data in the literature for the comparison with our results.

2. Experimental setup and plasma diagnostics

Measurements were performed in the pulsed arc plasma. Pulses were created by discharging a capacitor bank, charged up to 8.2 kV, through a cylindrical Pyrex tube. A mixture of krypton (8%) and helium (92%) was flowing continuously through the tube at a pressure of 2.6 kPa. The experimental set-up is described in detail in our previous papers [7, 8]. Electron density, determined by a two-wavelength laser interferometer method, was in the range $(0.7 - 2.0) \times 10^{23}$ m^{-3}. Error of the electron density measurements was estimated to be lower than 10%. Electron temperature, determined by the Boltzmann-plot, was in the range (16000 − 22000) K. Experimental uncertainty for this parameter was estimated to be lower than 15%.

3. Results and discussion

Measured Stark shifts of several Kr III spectral lines are given in Table 1. In the first three columns, the table contains configurations, terms and wavelengths of the observed spectral lines. In the next two columns, measured shifts, dm, and estimated accuracy, Acc., are presented. The multiplets notation is the same as in the NIST atomic spectra database [9]. Data are normalized to the electron density $N_e = 1 \times 10^{23}$ m^{-3} and the electron temperature $T_e = 18000$ K. The last column of the table contains the ratio between the measured and the calculated shifts, $d_{\rm m}/d_{\rm SMSE}$. Theoretical data were obtained from the simplified modified semi-empirical shift formula [10].

Table 1. Experimental Stark shifts, $d_{\rm m}$, normalized to electron density $N_e = 1 \times 10^{23}$ m^{-3} and electron temperature $T_e = 18000$ K. Estimated accuracy, Acc, is given in a separate column. Experimental results are compared with the theoretical data [10], $d_{\rm m}/d_{\rm SMSE}$.

No.	Configurations	Terms	Wavelength (nm)	$d_{\rm m}$ (pm)	Acc. (%)	$\frac{d_{\rm m}}{d_{\rm SMSE}}$
1.	$4s^24p^3(^4S^o)4d - 4s^24p^3(^4S^o)5p$	$^5D^o_1 - ^5P_2$	267.962	1.58	58	1.07
2.	$4s^24p^3(^2D^o)4d - 4s^24p^3(^2D^o)5p$	$^3F^o_4 - ^3D_3$	253.757	1.22	80	0.69*
3.		$^3F^o_4 - ^1F_3$	257.119	1.12	48	-
4.		$^3G^o_4 - ^1F_3$	289.368	2.11	37	0.91
5.	$4s^24p^3(^2D^o)5s - 4s^24p^3(^2D^o)5p$	$^3D^o_1 - ^3P_0$	281.448	- 2.20	49	0.69*
6.		$^3D^o_2 - ^3P_2$	290.004	- 2.47	27	0.72*
7.		$^1D^o_2 - ^3P_1$	299.660	2.34	38	0.88*
8.	$4s^24p^3(^2D^o)5s - 4s^24p^3(^2P^o)5p$	$^1D^o_2 - ^3P_1$	260.435	$\lvert d\rvert < 2$	-	-
9.	$4s^24p^3(^2P^o)4d - 4s^24p^3(^2D^o)5p$	$^3P^o_1 - ^3S_1$	280.607	$\lvert d\rvert < 2$	-	-
10.	$4s^24p^3(^4S^o)5p - 4s^24p^3(^4S^o)6s$	$^5P_3 - ^5S^o_2$	256.325	8.70	22	0.94

As already mentioned, in this experiment only low intensity lines were considered. As

an example, a part of the recorded spectrum is shown in Figure 1. In this figure, the profile of the 267.962 nm line is shown together with two more intense lines and another separated line. Similar situation is with other considered spectral lines.

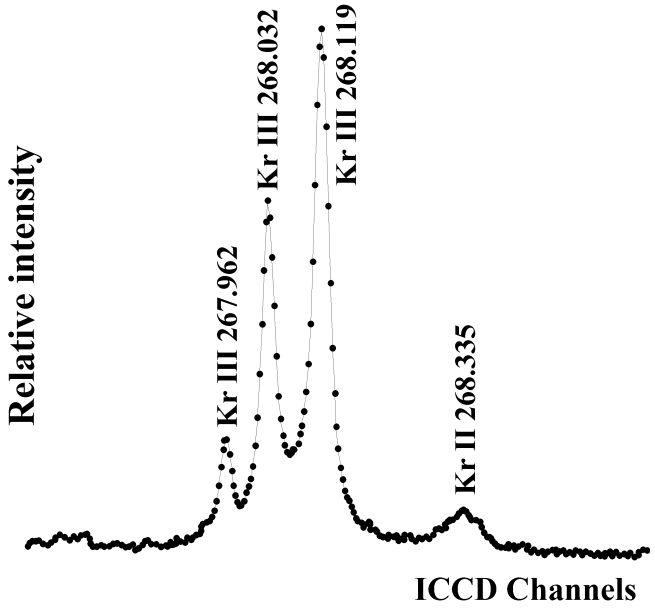

Figure 1. Part of the ionized krypton spectrum.

All spectral lines were checked on self-absorption effect, using an external mirror [8]. The chosen percentage of krypton in the krypton-helium mixture ensured the absence of self-absorption for all the lines taken into consideration.

Apart from taking care of experimental conditions and applied plasma diagnostics, attention was also paid to the proper fitting procedure. The spectra were fitted to the sum of Lorentzian functions (for spectral lines) and a linear function (for continuum emission) [11]. The deconvolution procedure used is described in [12].

Under these experimental conditions, Stark broadening is the dominant broadening mechanism. Two other pressure broadening mechanisms, resonance and van der Waals, were found to be negligible. Therefore, only Gaussian (instrumental + Doppler) and Stark broadening were taken into account in the deconvolution procedure.

Stark shift of the Kr III 267.962 nm line as a function of electron density is shown in Figure 2. Stark shifts were obtained using a method described in Aparicio et al. [13]. Firstly, it was assumed that there was no Stark shift when electron density was $N_e = 0$. Since the exact position of an observed spectral line at $N_e = 0$ is unknown, this value was obtained by extrapolating the linear fit of the lines center positions versus electron density to zero electron density. Once this value was subtracted from the measured lines center positions, the resulting differences multiplied by the inverse linear dispersion of the spectroscopic system gave us the measured Stark shift values (in pm) of the studied spectral lines.

All possible errors in the line shape recording, transmittance correction, as well as fitting and deconvolution procedure were included in the final experimental accuracy estimation given in Table 1. Relatively large experimental errors and consequently large

scatter of the experimental points (see Figure 2) are due to the low signal/noise ratio, since we deal with low intensity spectral lines. Furthermore, it is well known that Stark shift measurements are, in general, less accurate than Stark halfwidth measurements, especially in cases where shifts are very small.

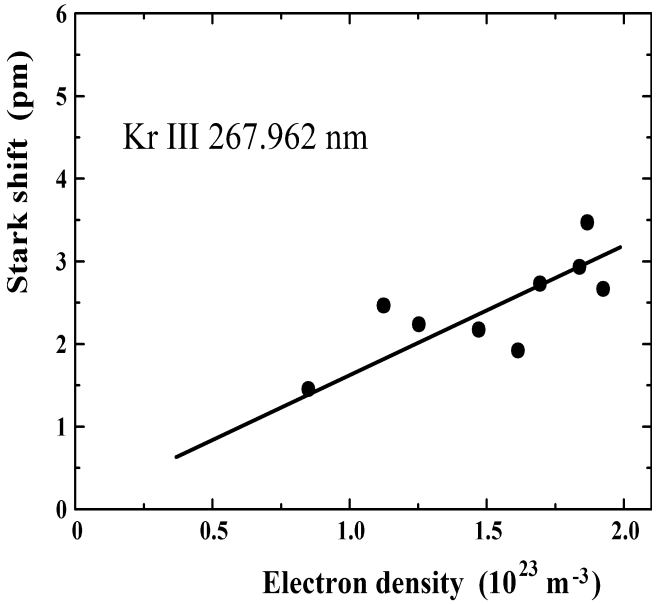

Figure 2. Example of Stark shift measurement.

In the 8th and 9th row of Table 1, shift results for the lines 260.435 nm and 280.607 nm are given in the form $|d| < 2$. This means that the measured shift is very small, practically null, while the dispersion of the points is within ±2 pm for these lines.

In cases where it was possible, experimental shift results were compared to the theoretical data obtained from the simplified modified semi-empirical shift formula [10]. The comparisons are given in the last column of Table 1. One should keep in mind that there is a certain restriction for using formula [10]. In order to use this formula, it is necessary that the nearest perturbing level $E_{j'}$ is situated far enough from the observed transition level E_j. This is expressed by the condition $E/\Delta E_{jj'} = 2$, where $E = 3kT/2$ is the energy of perturbing electron and $\Delta E_{jj'} = |E_j - E_{j'}|$. This condition is not satisfied for the 257.119 nm line, so the comparison is omitted. In the other four cases, where $d_{\mathrm{m}}/d_{\mathrm{SMSE}}$ ratio is denoted with asterisk, the necessary conditions for the calculations are at the upper limit. The $d_{\mathrm{m}}/d_{\mathrm{SMSE}}$ ratios vary between 0.69 and 1.07. This can be considered as a very good agreement, if one takes into account relatively large experimental errors and a fact that the shift formula [10] gives only rough shift estimations. The most important is that signs of the experimental and theoretical shifts are in agreement in all cases. It is obvious that the estimated values for the lines 260.435 nm and 280.607 nm could not be compared with the theoretical results.

Among the presented results, there is only one spectral line per multiplet and supermultiplet, so the Stark shifts regularity check can be done only for transition arrays. In Wiese and Konjevic [3] it was found that Stark shifts of the lines belonging to the same transition array normally have values within ±25%. In cases when the shift makes a relatively large fraction of the halfwidth, the variation is within approximately ±50%. Here,

we have a variation of Stark shifts from -26% to $+40\%$ around the average value, for $4d-5p$ transition array. Within the $5s-5p$ transition array there are different shift signs, which is also theoretically predicted (see Table 1).

The presented Stark shift data, in general, can be used for diagnostic purposes, demonstration of regularities and similarities of line shifts within the transition arrays or, by combining them with the future experimental results, within the multiplets or supermultiplets [3]. In addition, these results can be used for theory testing, and they are also of interest in astrophysics.

Acknowledgments

We thank S. González for his work on the experimental device, the Spanish Ministerio de Ciencia y Tecnologa and the Consejera de Educación y Cultura de la Junta de Castilla y Leon for their financial support under contracts No. $FIS2005-03155$ and $VA015A05$ respectively. Dr J. A. Aparicio wants to express his personal acknowledgement to the ONCE for help. S. Djurović thanks to the Ministry of Science and Development of the Republic of Serbia for support in Project No. 141024.

References

[1] M. A. Cayless and A. M. Marsden, in *Lamps and Lighting*, 3rd ed., (Edward Arnold, London, 1983).

[2] K. Shimoda, in *Introduction to Laser Physics*, (Springer Series in Optical Sciences Vol. 44, Springer, Berlin 1984).

[3] W. L. Wiese and N. Konjević, J. Quant. Spectrosc. Radiat. Transfer, **47**, 185 (1992).

[4] M. Ćirišan, R. J. Peláez, S. Djurović, J. A. Aparicio and S. Mar, Phys. Rev. A (in press).

[5] H. O. Di Rocco, G. Bertuccelli, J. Reyna Almandos, F. Bredice and M. Gallardo, J. Quant Spectrosc. Radiat. Transfer, **41**, 161 (1989).

[6] V. Milosavljević, S. Djeniže, M. S. Dimitrijević and L. Č. Popović, Phys. Rev. E **32**, 4137 (2000).

[7] J. A. del Val, S. Mar, M. A. Gigosos, M. I. de la Rosa, C. Pérez and V. R. González, Jpn. J. Appl. Phys. **37**, 4177 (1988).

[8] S. Djurović, R. J. Peláez, M. Ćirišan, J. A. Aparicio and S. Mar, J. Phys. B: At. Mol. Opt.Phys. **39**, 2901 (2006).

[9] NIST, Atomic spectra database, http:/physics.nist.gov./asd

[10] M. S. Dimitrijević and N. Konjević, Astron. Astrophys. **172**, 345 (1987).

[11] M. A. Gigosos, S. Mar, C. Pérez and M. I. de la Rosa, Phys. Rev. E **49**, 1575 (1994).

[12] J. T. Davies and J. M. Vaughan, Astrophys. J. **137**, 1302 (1963).

[13] J. A. Aparicio, C. Pérez, J. A. del Val, M. I. de la Rosa and S. Mar, J. Phys. B: At. Mol. Opt. Phys. **31**, 4909 (1998).

Journal of Research in Physics Vol. 34, No. 1, 39 - 45 (2010)

Chemical stability of glassy $Sb_xAs_{37-x}S_{48}I_{15}$ chalcohalides

Goran Štrbac, Svetlana Lukić-Petrović, Imre Gut, Dragana Štrbac,
Faculty of Sciences, Department of Physics,
Trg Dositeja Obradovica 4, 21000 Novi Sad, Serbia
Spyros N. Yannopoulos
Foundation for Research and Technology Institute of Chemical Engineering and High Temperature Chemical Processes (FORTH/ICE-HT),
P.O. Box 1414, GR-26504, Rio-Patras, Greece

Received: *December 10, 2010*

Abstract

The paper describes results of the research carried out with the aim of establishing chemical stability of the glasses of the $Sb_xAs_{37-x}S_{48}I_{15}$ type.
Samples were synthesized and investigated in order to determine the influence of the substitution of As atoms with Sb atoms on thermally induced SbSI ferroelectric centers.
Chemical stability of glasses was estimated on the basis of their dissolution rate in potassium hydroxide solution of different concentrations. It was found that the rate of dissolution decreases with the increase of antimony content in the glass. The dissolution rate also depends on the concentration of the basic solution. It was found that the dependence of the dissolution rate on time and on base concentration can be described satisfactorily by an exponential function.

Key words: glasses, chalcohalides, dissolution rate, chemical stability

1. Introduction

The unique properties of chalcogenides, which are different from those of oxide and halide glasses, have led to a long-term high scientific and industrial interest. Investigations of mechanical, electrical, optical and other physical properties of amorphous semiconducting materials have shown that these properties depend substantially on the system composition. The addition of halides leads to the formation of chalcohalide glasses with new features. Four- and five-component systems show exceptional potential regarding the possibility of modifying selected properties relevant to applications in a desired way. This results from the strong influence of materials properties on chalcogenide glass composition [1-4].

The current study focuses on the investigation of the ternary system $Sb_xAs_{37-x}S_{48}I_{15}$ for $x = 0$, 7 and 22 at%. The primary goal is to determine the influence of the substitution of As atoms with Sb atoms on thermally induced SbSI ferroelectric centers, i.e. on selected

ferroelectric characteristics of glass-ceramics material (sital). It is known that SbSI can be obtained in (partially) amorphous phase only under special conditions [5]. On the other hand, the presence of arsenic is expected to improve the amorphization process of the above ferroelectric system.

The possibility that such materials could find viable applications is determined and limited by their stability to various aggressive media. However, even the lower stability in some reagents provides those chalcohalide materials certain advantages including: the possibility of relief formation, removal of the surface layer and impurities by surface treatment, enhancement of the optical contrast of amorphous films in the amplitude-phase storage of optical information, surface preparation for metallographic examination, etc.

It has been shown that complex amorphous chalcogenides, in general, exhibit chemical stability under ambient conditions; they are not hygroscopic and exhibit high chemical stability with respect to most aggressive media. They do not interact with most acids and dissolve very slowly in dilute nitric acid. However, they are less stable in basic solutions and some solvents containing amino groups [6-9].

2. Experimental

The investigated glasses were synthesized from high-purity elements (99.99%). The synthesis was carried out according to a method published elsewhere [10].

The experiments were performed in several stages. First of all, masses before treatment in the basic solution and dimensions of prepared samples were measured, and then they were treated in a basic solution of chosen concentration. Every ten seconds chemical reaction was stopped by sinking the sample into distilled water. Then, the samples were dried and their mass and dimensions were measured again. The procedure was successively repeated ten times.

The rate of sample dissolution in a chemical reagent at various concentrations was determined by an indirect method via weight loss, using the following equation:

$$\mathrm{w} = \frac{\Delta m}{SM\Delta M} \qquad [\mathrm{mol\ m^{-2}s^{-1}}] \tag{1}$$

where Δm is the mass change during the dissolution time Δt, S is the sample surface and M is the molecular mass of the conditional chemical unit. Samples were polished mechanically, using carborundum powder of different grain fineness ($260 - 28$ mm) to obtain regular geometric shapes (rectangle, cube). The chemical stability of glasses was estimated on the basis of their dissolution rate in potassium hydroxide at concentrations 0.5 mol $\mathrm{dm^{-3}}$ (0.5 M), 1 mol $\mathrm{dm^{-3}}$ (1 M) and 2 mol $\mathrm{dm^{-3}}$ (2 M). The estimated accuracy of dissolution rate is $5 - 10\%$. Samples with 0, 7 and 22 at% of antimony have been investigated.

Since previous investigations [11, 12] showed that the stirring of the solution has only a weak influence on the rate of dissolving of chalcogenide non-crystalline semiconductors, it can be considered that the dissolving of chalcogenides in basic media is primarily governed by the rate of heterogeneous chemical reaction on the sample surface.

This assumption enables the calculation of the dissolution rate of glasses of certain compositions using Equation (1), where the change on the sample surface and the weight loss are experimentally determined. During the dissolution experiments, the color of the

basic solution was gradually changing from dark red to gray, depending on the chalcohalide composition and the concentration of the base solution.

On the basis of the performed experiments, it was possible to determine the functional dependence of the weight loss and change of the sample surface. The change of the sample surface during the treatment with the aggressive media can be described by a linear function with an accuracy which does not exceed the errors of directly measured values. The mass change of the treated chalcohalide samples with time can be described by a very weak exponential function.

3. Results and discussion

Representative curves showing the dependence of the dissolution rate on time for selected samples from the $Sb_xAs_{37-x}S_{48}I_{15}$ system for different concentration of the base, at room temperature, are shown in Figures 1-3.

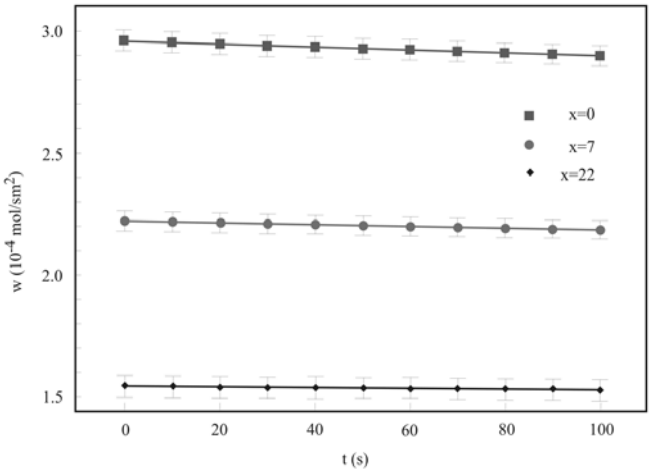

Figure 1. Dependence of the dissolution rate on time of $Sb_xAs_{37-x}S_{48}I_{15}$ glasses in 0.5 M KOH.

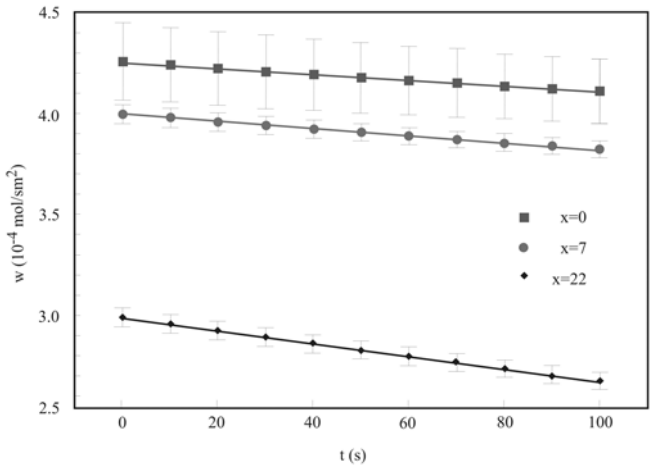

Figure 2. Dependence of the dissolution rate on time of $Sb_xAs_{37-x}S_{48}I_{15}$ glasses in 1 M KOH.

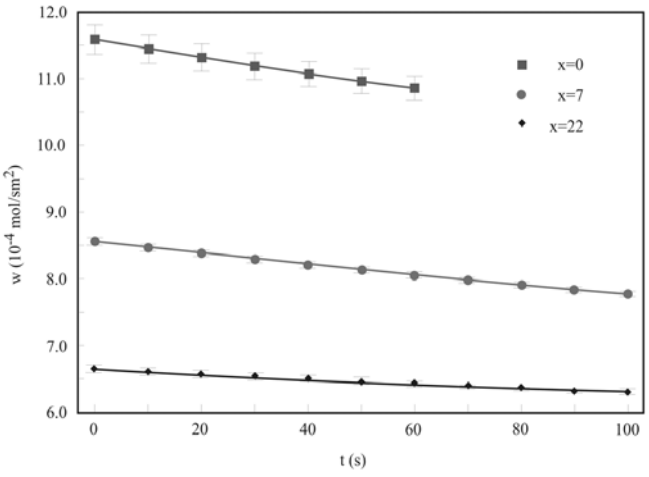

Figure 3. Dependence of the dissolution rate on time of $Sb_xAs_{37-x}S_{48}I_{15}$ glasses in 2 M KOH.

Dissolution rates in 0.5 M basic solution, for the sample without antimony, ranged from $2.96 \cdot 10^{-4}$ mol m^{-2} s^{-1} to $2.89 \cdot 10^{-4}$ mol m^{-2} s^{-1} and for the sample with 22 at% of antimony vary from $1.55 \cdot 10^{-4}$ mol m^{-2} s^{-1} to $1.53 \cdot 10^{-4}$ mol m^{-2} s^{-1}. The values of dissolution rate in 2 M basic solutions were in the range from $11.59 \cdot 10^{-4}$ mol m^{-2} s^{-1} to $10.85 \cdot 10^{-4}$ mol m^{-2} s^{-1} for the sample without antimony and in the range from $6.61 \cdot 10^{-4}$ mol m^{-2} s^{-1} to $6.26 \cdot 10^{-4}$ mol m^{-2} s^{-1} for the sample with 22 at% of antimony.

The three investigated samples have shown a relatively low dissolution rate and the possibility of good control of the dissolution process for all three concentrations of potassium hydroxide. Time dependence measurements have shown that the dissolution rate decreases with time, which leads to a significant saturation of the basic solution in which the samples were treated. Based on this finding, as well as on related observations of similar chalcogenide glasses [12, 13], we have chosen to account for the observed time dependence fitting the experimental data with the aid of an exponential function. As already mentioned, in this experiment only low intensity lines were considered. As an example, a part of the recorded spectrum is shown in Figure 1. In this figure, the profile of the 267.962 nm line is shown together with two more intense lines and another separated line. Similar situation is with other considered spectral lines.

The dependence of the dissolution rate of glasses of the $Sb_xAs_{37-x}S_{48}I_{15}$ type on the base concentration is shown in Figure 4, for $t = 50$ s. As could be expected, it is clear that the dissolution rate increases with increase of basic solution concentration and that the dependence is of an exponential type.

Dependence of the dissolution rate on the antimony content in the glass composition during the dissolution time of $t = 50$ s for different KOH concentrations is shown in Figure 5. On the basis of the experimental data it was possible to describe this functional dependence by a monotonic function. It may be noticed that the dissolution in 2 M KOH exhibits significantly larger change in the dissolution rate with the change in the structural composition compared with the more dilute solutions.

The dissolution rate decreases with the increase of atomic percentage of antimony in the investigated materials, so it can be concluded that this element has a positive effect on the chemical stability of the chalcogenide sample.

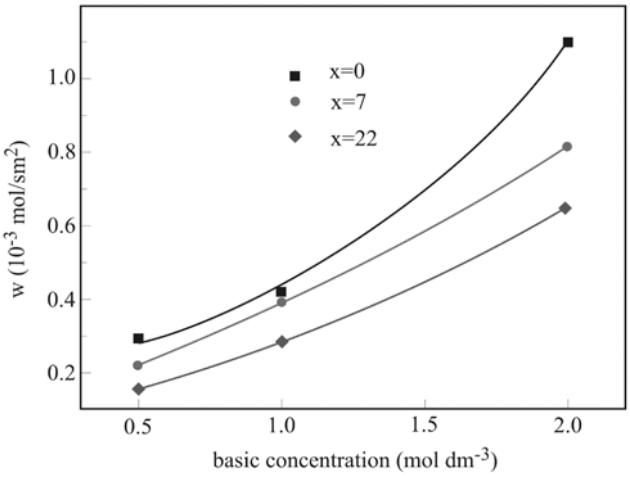

Figure 4. Dependence of the dissolution rate on the basic concentration of $Sb_xAs_{37-x}S_{48}I_{15}$ glasses.

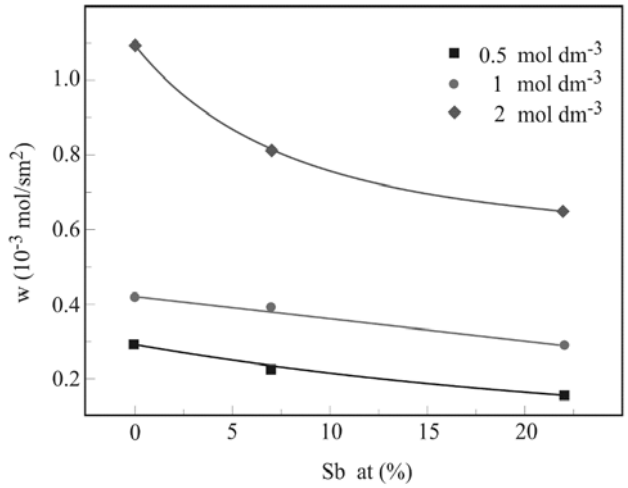

Figure 5. Dependence of the dissolution rate of $Sb_xAs_{37-x}S_{48}I_{15}$ glasses on the antimony content.

This can be explained by the changes in the ionic-covalent share of bonds and by the fact that the changes in the glass composition cause changes in the population of certain structural units in the glass matrix. Previous results have shown that the dissolution of binary amorphous As_2S_3 system is related to the capability of As and S atoms to form anions of variable composition [14]. This binary amorphous system has a polymeric chain structure made of As_2S_3 trigonal pyramidal units, with each arsenic atom surrounded by three sulfur atoms [15]. A first step in the dissolution of these systems is the breaking of the polymeric bonds $-S-As<$, and separation of the structural ring $-S-As<\begin{matrix}S\\S\end{matrix}>As-$ from the polymeric molecule, which then enters a chemical reaction with the molecules of the basic solution.

It is supposed that in the As−S−I glasses there are polymeric chains $(-S-S-)_n$ and the iodine plays the role of a chain terminator. The structure can be regarded as a network of

As_2S_3 pyramids interconnected by simple or double sulfur bridges or by −S−S− units. The network would contain molecular species dissolved: S_8, AsI_3, etc. [16]. The introduction of antimony instead of arsenic does not change the basic structure drastically because Sb is an element analogous to As, as an element from the same group of the periodic table of elements. They form similar structural units such as $As_2S_3(Sb_2S_3)$, AsSI(SbSI), etc. However, antimony raises the metallic character of the chemical bond in the system. The Sb−S−I bonds are weaker than Sb−S bonds, as well as As−S−I compared to As−S, because iodine increases the ionic contribution in the chemical bond [16].

Results of studying chemical stability study have shown the usual behavior of dissolution of the glasses from the investigated system in the basic solutions with specified concentrations, and, accordingly, can be used for relief formation at surfaces after proper photoinduced treatment.

4. Conclusion

The solubility of samples from the Sb−As−S−I system is determined by the rate of the heterogeneous chemical reaction on the sample surface. The functional dependence of the dissolution rate on time has been determined. The dissolution rate decreases with increase of the antimony content in the glass. This parameter also depends on the concentration of the basic solution. All three investigated samples have shown a relatively low dissolution rate at the concentrations of the basic solutions used and, consequently, the dissolution process can be well controlled for all three investigated basic solutions.

Acknowledgments

The work was partly financed by the Provincial Secretariat of Science and Technological Development, Autonomous Province of Vojvodina, in the frame of the project *"Technology of obtaining and characterization of disordered semiconductors"*.

References

[1] S. R. Lukić, D. M. Petrović, D. D. Štrbac, V. B. Petrović, F. Skuban, J. Therm. Anal. Cal., **82**, 41, (2005).

[2] A. Thakur, V. Sharma, G. S. S. Saini, N. Goyal, S. K. Tripathi, J. Optoel. Adv. Mat., **7**, 2077, (2005).

[3] I. Ohlídal, D. Franta, M. Frumar, J. Jedeleský, J. Omasta, Chalc. Lett., **1**, 1, (2004).

[4] A. K. Pattanaik, A. Srinivasan, J. Optoel. Adv. Mat., **5**, 1161, (2003).

[5] G. Z. Vinogradova, *Stekloobrazovanie i fazovye ravnovesiya v hal'kogenidnyh sistemah*, (Nauka, Moskva, 1984).

[6] Z. U. Borisova, *Himiya stekloobraznyh poluprovodnikov*, (LGU, Leningrad, 1972).

[7] Ya. A. Ugaj, *Vvedenie v himiyu poluprovodnikov*, (Vysshaya shkola, Moksva, 1977).

[8] M. Brodski, *Amorfnye poluprovodniki*, (Mir, Moskva, 1982).

[9] V. I. Vlasov, D. G. Semak, D. B. Chepur, ser. Fizika, VUZov, **12**, 48, (1978).

[10] G. R. Štrbac, F. Skuban, S. R. Lukić, D. D. Štrbac, J. Optoel. Adv. Mat., **6**, 1690, (2007).

[11] S. R. Lukić, Ž. N. Popović, J. Janjić, I. Guth, Balkan Phys. Lett., **5**, 868, (1997).

[12] D. B. Mijatović, Ž. N. Popović, J. Janjić, F. Skuban, M. I. Avramov, J. Res. Phys., **28**, 81, (1999).

[13] S. R. Lukić, D. M. Petrović, G. R. Štrbac, A. F. Petrović, M. Šiljegović, J. Phys. Chem. Solids **66**, 1683, (2005).

[14] S. V. Svechnikov, V. V. Himinec, N. I. Dovgoshei, *Slozhnye nekristallicheskie hal'kogenidy i hal'kogalogenidy i ih primenenie v optoelektronike*, (Naukova dumka, Kiev, 1992).

[15] G. Lucovsky, R. M. Martin, J. Non-Cryst. Solids, **8**, 185, (1972).

[16] M. A. Popescu, *Non-crystalline Chalcogenides*, (National Institute of Materials Physics, Bucharest, 2002).

Journal of Research in Physics

INFORMATION FOR CONTRIBUTORS

This Journal is devoted to the publication of original papers in **fundamental and applied physics**. The papers are in principle Articles, while Review Articles will be published by invitation only.

Contributors should send their manuscripts to Professor M. Škrinjar, Editor, Department of Physics, Faculty of Sciences, University of Novi Sad, Trg Dositeja Obradovića 4, 21000 Novi Sad, Serbia. (Fax #:+381-(21)-459-367; E-mail: jresphys@df.uns.ac.rs).

All manuscripts must be submitted in English. Manuscripts should be submitted in duplicate and should be typewritten and double spaced with wide margins. Only one side of each sheet should be used.

Manuscripts should consist of the title, followed by author(s) name(s) and adresse(s), abstract, key words, body of the text and the list of the references. Authors should *not* include references in Abstracts.

References must be numbered in the order in which they are referred to in the text: e.g. S. Wagner [1] or [1]. In the text, such abbreviations as Ref. [4] or Refs. [7-10] may be used.

The full references should be listed in the numerical order of citation in the text at the end of the article. Examples:

1. S. Autler and C. H. Townes, Phys. Rev. A **10**, 489 (1982). – for articles
2. E. U. Shirley, *The Theory of Molecules*, p. 399, (The University Press, Cambridge, 1954). – for books
3. C. E. Moore, "Selected Tables of Atomic Spectra", NSRDS-NBS3, Setion 5, National Bureau of Standards, Washington, DC 20025 (1975). – for reports.

Tables and figures should be sent with the paper on the separate pages. All photographs, graphs, and diagrams should be numbered consecutively. The legends should be typed on a separate page at the end of the article. The author's name, the figure number, and an indication of its proper orientation should be written on the back of each figure.

Line drawings must be submitted in camera-ready form and should be drawn in india ink on stiff white paper or printed on quality laser printer. The letters and symbols should be drawn so as to be clearly legible when reduced.

Authors are asked to suggest at least three referees who may revise their manuscript.

Page proofs will be sent to the author (or the first-mentioned author in a paper of multiple authorship) for checking. **Corrections to the proofs must be restricted to printer's errors**. Authors are particularly requested to return their corrected proofs as quickly as possible. Please note that **authors are urged to check their proofs carefully before return, since late corrections cannot be guaranteed for inclusion in the printed journal.**

The first-named author of each paper will receive 25 reprints free of charge.

Journal of Research in Physics

Volume 34 Number 1 December 2010

CONTENTS